Dear Dr. Reverdin,

We thank you for handling our manuscript. We have addressed your comments and made minor revisions detailed below in blue font.

Best regards,

Yi Tang on behalf of all authors

"I have just read the new posted replies to the reviews.

Overall, I find that you are doing a good job in taking them into account, and that the proposed changes respond well to the comments posted. There is just one part that left me somewhat puzzled (here, I cite it from the reply to reviewer 2):

... the uncertainty of the 210Po export flux was on average 2-fold larger than the value of 210Po export flux. When the uncertainty propagated from all the variables mentioned above confirms that our estimates are the right order of magnitude, we feel justified in publishing the results, and confident...

2-fold for me means 'double'... If that's correct, I understand that the uncertainty is twice the export flux. Thus it implies that one is not sure of even the sign of the export flux. This might be the case (except if I misunderstood the statement), but reading the abstract, I got the feeling that the results were more certain than that.

So, if I understood correctly and based on these changes in the manuscript, I believe that it is necessary to modify slightly the abstract and that referring to this careful estimate of the uncertainty might be warranted."

We acknowledge that the uncertainty of the ^{210}Po export flux is large due to the large variance in vertical velocity. As you say, the uncertainty is 2-fold larger. And it indeed means that one is not sure of the sign of the export flux.

We will modify "The deficit of ^{210}Po in the Iberian Basin and at the Greenland Shelf were strongly affected by vertical advection" in the Abstract as:

"Vertical advection was incorporated into one version of the model using time-averaged vertical velocity, which had substantial variance. This resulted in large uncertainties for the ^{210}Po export flux in this model, suggesting that those calculations of ^{210}Po export fluxes should be used with great care. Despite the large uncertainties, there is no question that the deficits of ^{210}Po in the Iberian Basin and at the Greenland Shelf have been strongly affected by vertical advection along the transect."

1 **The export flux of particulate organic carbon derived from [210]Po/^{210}Pb disequilibria along**

2 **the North Atlantic GEOTRACES GA01 ~~(GEOVIDE)~~ transect: GEOVIDE cruise**

3

4 Yi Tang[1,2], Nolwenn Lemaitre[3], Maxi Castrillejo[4,5], Montserrat Roca-Martí[5,6], Pere Masqué[5,7],

5 Gillian Stewart[2,1]

6

7 [1] Earth and Environmental Sciences, the Graduate Center, City University of New York, New York, USA

8 [2] School of Earth and Environmental Sciences, Queens College, City University of New York, Flushing, USA

9 [3] Department of Earth Sciences, Institute of Geochemistry and Petrology, ETH-Zürich, Zürich, Switzerland

10 [4] Laboratory of Ion Beam Physics, ETH-Zürich, Otto Stern Weg 5, Zürich, 8093, Switzerland

11 [5] Institut de Ciència i Tecnologia Ambientals and Departament de Física, Universitat Autònoma de Barcelona,

12 Barcelona, Spain

13 [6] Woods Hole Oceanographic Institution, Woods Hole, MA 02543, USA

14 [7] School of Science and Centre for Marine Ecosystems Research, Edith Cowan University, Joondalup, Western

15 Australia, Australia

16

17 Correspondence to: Gillian Stewart (Gillian.Stewart@qc.cuny.edu)

18

19

Abstract

The disequilibrium between ^{210}Po activity and ^{210}Pb activity in seawater samples was determined along the GEOTRACES GA01 transect in the North Atlantic during the GEOVIDE cruise (May – June 2014). A steady-state model was used to quantify vertical export of particulate ^{210}Po. Vertical advection was incorporated into one version of the model using time-averaged vertical velocity, which had substantial variance. This resulted in large uncertainties for the ^{210}Po export flux in this model, suggesting that those calculations of ^{210}Po export fluxes should be used with great care. Despite the large uncertainties, there is no question that the The deficits of ^{210}Po in the Iberian Basin and at the Greenland Shelf have been were strongly affected by vertical advection. Using the export flux of ^{210}Po and the particulate organic carbon (POC) to ^{210}Po ratio on total (> 1 μm) particles, we determined the POC export fluxes along the transect. Both the magnitude and efficiency of the estimated POC export flux from the surface ocean varied spatially within our study region. Export fluxes of POC ranged from negligible to 10 mmol C m^{-2} d^{-1}, with enhanced POC export in the Labrador Sea. The cruise track was characterized by overall low POC export relative to net primary production (export efficiency < 1-15%); but relatively high export efficiencies were seen in the basins where diatoms dominated the phytoplankton community. The particularly low export efficiencies in the Iberian Basin, on the other hand, were explained by the dominance of smaller phytoplankton, such as cyanobacteria or coccolithophores. POC fluxes estimated from the ^{210}Po/^{210}Pb and ^{234}Th/^{238}U disequilibria agreed within a factor of 3 along the transect, with higher POC estimates generally derived from ^{234}Th. The differences were attributed to integration timescales and the history of bloom events.

1. Introduction

The oceans play an essential role in the regulation of atmospheric CO_2 and the buffering of the global climate system (e.g. Sabine, 2004) by removing carbon from the atmosphere via dissolution and photosynthesis in the surface ocean, and storing it in the dissolved or particulate forms. An important component of this oceanic sequestration is the biological carbon pump, driven by sinking particles from the surface to the deep ocean (e.g. Falkowski et al., 1998; Ducklow et al., 2001).

The magnitude of particulate organic carbon (POC) export flux from the upper ocean was traditionally obtained from time-series sediment traps (e.g. Honjo et al., 2008) and the natural radiotracer pair, $^{234}Th/^{238}U$ (e.g. Bhat et al., 1968; Buesseler et al., 1992). Here we focus on the application of another natural radionuclide pair: polonium-210 (^{210}Po, $T_{1/2} = 138.4$ d) and its progenitor lead-210 (^{210}Pb, $T_{1/2} = 22.3$ y). The $^{210}Po/^{210}Pb$ pair has a different particle-binding dynamic compared to the $^{234}Th/^{238}U$ pair since both isotopes are particle-reactive, whereas ^{238}U is conservative and remains dissolved in seawater (Djogic et al., 1986). However, the nature of the particle association differs between the isotopes. Lead-210 and ^{234}Th are only adsorbed to particle surfaces, whereas ^{210}Po is both adsorbed to surfaces and biologically reactive so can be assimilated by organisms and even bioaccumulated (Fisher et al., 1983; Cherrier et al., 1995; Stewart and Fisher, 2003a; 2003b). This behavior leads to a higher partitioning coefficient (relative association between the isotope and the particulate vs. the dissolved phase) of ^{210}Po compared to that of ^{210}Pb (e.g. Masqué et al., 2002; Wei et al., 2014; Tang et al., 2017).

Lead-210 in the water column comes both from atmospheric deposition and in situ production via the decay of ^{226}Ra. The residence time of ^{210}Pb in the atmosphere is only days to weeks (Moore et al., 1974; Turekian et al., 1977). Polonium-210 (produced by decay of ^{210}Pb via ^{210}Bi) activities in aerosols, and the subsequent fluxes to the surface ocean, are only about 10 – 20% those of ^{210}Pb (Masqué et al., 2002). The large difference in their particle reactivity, and half-lives, and the original $^{210}Po/^{210}Pb$ activity ratio in the aerosols often leads to a disequilibrium between ^{210}Po and ^{210}Pb activities in the upper water column as particles sink.

This deviation from secular equilibrium, often in the form of a deficit of ^{210}Po activity with respect to ^{210}Pb activity, can be used to estimate POC export in a similar manner to the application of the $^{234}Th/^{238}U$ disequilibrium (Friedrich and Rutgers van der Loeff, 2002; Verdeny et al., 2009; Wei et al., 2011). Particle export fluxes estimated from the $^{234}Th/^{238}U$ and the

74   ^{210}Po/^{210}Pb disequilibria integrate export that has occurred on time scales of weeks to months

75   prior to the sampling time, respectively. The use of both isotope pairs could provide

76   complementary information on the causes, timing, and efficiency of export fluxes of POC (e.g.

77   Murray et al., 2005; Stewart et al., 2007; Roca-Martí et al., 2016).

78   In this study along the GEOTRACES GA01 transect in the North Atlantic, we first used a

79   traditional scavenging model with the assumptions of steady state and negligible physical

80   transport to derive ^{210}Po fluxes over different depths of the water column at 11 stations. Then,

81   vertical advection (primarily upwelling) was considered, and its impact on ^{210}Po flux was

82   assessed. Using the POC concentration, and particulate ^{210}Po activity in the ~~pumped~~ particles

83   collected by in situ pumps, sinking fluxes of POC were then calculated. The magnitude and

84   efficiency of carbon export derived from the ^{210}Po/^{210}Pb disequilibrium was considered in

85   relation to the composition of the phytoplankton community. Finally, the POC export fluxes

86   estimated from ^{210}Po/^{210}Pb disequilibria were compared with those derived from ^{234}Th/^{238}U

87   disequilibria.

88

89   **2. Methods**

90   **2.1. Cruise track and hydrographic setting**

91   The GEOVIDE cruise (GEOTRACES GA01 transect) was carried out in May - June 2014

92   from Lisbon to Newfoundland (Fig. 1). Seawater and particulate samples for ^{210}Po and ^{210}Pb

93   activity analysis were collected from the water column at 11 stations (Fig. 1). The GA01 transect

94   can be separated into five sections according to their biogeochemical characteristics, described in

95   detail by Lemaitre et al., (2018). From east to west, these are: the Iberian Basin (stations 1, 13),

96   the Western European Basin (stations 21, 26), the Iceland Basin (stations 32, 38), the Irminger

97   Basin (stations 44, 60), and the Labrador Basin (stations 64, 69, 77).

98

99   **2.2. Radionuclides sampling and analysis**

100   Radionuclide data were produced by two collaborating laboratories to ensure higher counting

101   statistics for ^{210}Po activity in the samples: the Laboratori de Radioactivitat Ambiental at

102   Universitat Autònoma de Barcelona (UAB) (samples from stations 1, 13, and 21) and the Stewart

103   Laboratory at Queens College (QC) (samples from stations 26, 32, 38, 44, 60, 69, and 77). The

104   sampling method for total and particulate ^{210}Po and ^{210}Pb samples and the determination of the

4

radionuclides activities were described in Tang et al., (2018). In brief, water samples (5 – 10 L each) for total [210]Po and ^{210}Pb activity were collected using Niskin bottles at 10 full water column stations (16 – 22 depths/station) and at 1 station to 1000 m (9 depths), for a total of 200 samples. Particulate [210]Po and ^{210}Pb were collected at 3 – 10 depths per station between 15 and 800 m by using McLane in-situ pumps equipped with a 53 μm PETEX screen to capture the large size particles and a 1 μm quartz fiber QMA filter to capture small particles. The average equivalent volume filtered for particulate [210]Po and ^{210}Pb samples through the PETEX screen was 200 L and through the QMA filter was 70 L.

For water samples, Po and Pb isotopes (including the added chemical yield tracers of [209]Po and stable lead) were co-precipitated with cobalt-ammonium pyrrolidine dithiocarbamate (Co-APDC) (Fleer and Bacon, 1984) at sea, but digested using concentrated HCl and HNO$_3$ back at the home laboratories. Particulate samples were spiked with [209]Po and stable lead before acid digestions (UAB: HNO$_3$/HCl/HF, QC: HNO$_3$/HCl). Polonium isotopes ([209]Po and [210]Po) were plated by deposition onto a sliver disc (Flynn, 1968) and their activities were determined by alpha spectrometry. After removing any remaining Po isotopes by running the plating solution through an anion exchange column, the solution was respiked with [209]Po and stored for at least 6 months. Lead-210 activity was determined by plating the ingrowth of [210]Po from [210]Pb.

The activities of [210]Po and ^{210}Pb at the sampling date were determined by correcting for nuclide decay, ingrowth, chemical recoveries, detector backgrounds, and blank contamination (Rigaud et al., 2013).

2.3. The [210]Po flux method

The export flux of [210]Po was estimated from total [210]Po and ^{210}Pb activities using a one-box model (Broecker et al., 1973; Matsumoto, 1975; Savoye et al., 2006). The [210]Po activity in the surface ocean is the result of a balance between atmospheric input, continuous production from the decay of ^{210}Pb in seawater, radioactive decay of [210]Po, removal onto sinking particles, and transport into or out of the box by advection and diffusion. Therefore, the general form of the mass balance equation for [210]Po between sources and sinks is:

$$\partial Po / \partial t = F_{Po} + \lambda_{Po} I_{Pb} - \lambda_{Po} I_{Po} - P + V, \qquad \text{Eq. (1)}$$

136   where $\partial Po/\partial t$ is the change in ^{210}Po activity with time, F_{Po} (dpm m^{-2} d^{-1}) is the atmospheric flux

137   of ^{210}Po to the sea surface, λ_{Po} is the decay constant of ^{210}Po (0.005 d^{-1}), I_{Pb} and I_{Po} (dpm m^{-2})

138   are the inventories of ^{210}Pb and ^{210}Po activities, respectively, P (dpm m^{-2} d^{-1}) is the removal flux

139   of ^{210}Po via sinking particles, and V (dpm m^{-2} d^{-1}) is the sum of the advective and diffusive

140   fluxes.

141   The atmospheric flux of ^{210}Po is usually ignored as it represents only $\sim 2\%$ of the in-situ

142   production of ^{210}Po from ^{210}Pb in the upper water column of the open ocean (e.g. Cochran, 1992;

143   Masqué et al., 2002; Murray et al., 2005; Verdeny et al., 2008). We first used a steady state (SS)

144   model that assumes the negligible atmospheric input of ^{210}Po activity and ignores advection and

145   diffusion. In this case, the ^{210}Po flux (P) can be simplified as follows:

146

147    $P = \lambda_{Po}(I_{Pb} - I_{Po}).$ Eq. (2)

148

149   The influences of advection and non-steady state (NSS) processes on the overall ^{210}Po activity

150   balance are discussed below in sections 4.1 and 4.2, respectively.

151   Many previous studies have used a single fixed integration depth for export calculations at all

152   sampling locations (e.g. 100 m in the Antarctic Circumpolar Current, Rutgers van der Loeff et al.,

153   1997; 120 m in the central Equatorial Pacific, Murray et al., 2005). The GA01 transect, however,

154   crossed diverse physical and biogeochemical conditions. Thus, investigating export at a single

155   fixed depth for every station may bias the spatial comparisons of particle export. In this study,

156   four site-specific integration depths were used for each station: the mixed layer depth (MLD), the

157   depth of the euphotic zone ($Z_{1\%}$), the primary production zone (PPZ), and the ^{234}Th-^{238}U

158   equilibrium depth (ThEq). MLD ~~which~~ was defined as a change in potential density of 0.03 kg

159   m^{-3} relative to the potential density at 10 m (Weller and Plueddemann, 1996). ~~the depth of the~~

160   ~~euphotic zone ($Z_{1\%}$) which~~ was defined as the depth where photosynthetic available radiation

161   was 1% of its surface value (Jerlov, 1968).~~; the primary production zone (~~PPZ~~),~~ was the depth at

162   which the fluorescence reaches 10% of its maximum (Owens et al., 2015). ~~and the ^{234}Th-^{238}U~~

163   ~~equilibrium depth,~~ ThEq was the depth at the bottom of the total ^{234}Th water column deficit,

164   where the activity of ^{234}Th equals that of ^{238}U (data from Lemaitre et al., 2018), both to calculate

165   ^{210}Po and POC export and in order to compare the POC export fluxes estimated from the

166   ^{210}Po/^{210}Pb disequilibria to those derived from the ^{234}Th/^{238}U disequilibria. Among the 11

167   stations, the depths of the MLD (23 ± 7 m) were similar to those at $Z_{1\%}$ (31 ± 9 m), whereas the

168   depths of the PPZ (72 ± 29 m) and ThEq (95 ± 43 m) were deeper and comparable to each other.

169   For the depths of MLD, $Z_{1\%}$, PPZ, and ThEq at which total radionuclides data are not available,

170   the measured values of total ^{210}Po and ^{210}Pb activities were linearly interpolated ~~for the missing~~

171   ~~depths~~ (Table 1).

172   The ^{210}Po flux was then used to derive the flux of POC by multiplying the deficit of ^{210}Po by

173   the ratio of POC concentration to ^{210}Po activity (POC/^{210}Po) of the total particulate material.

174   Particulate ^{210}Po and POC data were not always available at the depths of the MLD, $Z_{1\%}$, PPZ,

175   and ThEq at our study sites. To ~~facilitate the~~ estimate ~~determination of~~ POC/^{210}Po ratios at these

176   depths, a regression was performed between the measured POC/^{210}Po ratios ~~grouped into 5~~

177   ~~basins as discussed above~~ and depth for each basin using a single power law function.

178

179   **2.4. Quantification of the influence of the vertical advection on ^{210}Po export**

180   Cyclonic/anticyclonic eddies constantly impact the horizontal velocity fields at our study

181   ~~sties~~ sites (Zunino et al., 2018), changing the current directions and making it difficult to

182   estimate the magnitude of horizontal velocities. This constant variability, together with the

183   patchiness of sampling resolution, which was not high enough to assess the influence of

184   horizontal advective processes on ^{210}Po export estimates~~, meant we did not attempt to quantify~~

185   ~~the horizontal advective flux of ^{210}Po activity~~.

186   However, because we had relatively high depth resolution at each station, we did attempt to

187   assess the influences of vertical advection on ^{210}Po inventories at all the investigated depths by

188   measuring the vertical gradient of ^{210}Po activity and multiplying it by a time-averaged ~~modeled~~

189   vertical velocity. Because the water column inventory of ^{210}Po represents an integration of the

190   changes over approximately the mean life of the isotope, we did not use the vertical velocity

191   measured by the acoustic doppler current profiler (ADCP) at the sampling time, but a time-

192   averaged vertical velocity from the Estimating the Circulation and Climate of the Ocean, Phase

193   II (ECCO2). The activity gradient of ^{210}Po below the depth z (i.e., the MLD, z1%, PPZ, and

194   ThEq) at each station was calculated from the depth z (using the average activity in the layer of

195   0-z m) as starting point (A_{Po}^{1}) and linearly interpolated through the measurements 20 m below z

196   (A_{Po}^{2}) at each station. A positive gradient ($A_{Po}^{2} - A_{Po}^{1} > 0$) was defined as higher activity at the

197   depth of ($z + 20$ m) than the starting point. We labeled the vertical velocity as w_{20} which was the

198 30-day (30 days prior to the sampling date) average vertical velocity between the depths of z and

199 $(z + 20 \text{ m})$. The flux of ^{210}Po due to vertical advection (F_w) was calculated as the following:

200

201 $F_w = w_{20} \times (A_{Po}^2 - A_{Po}^1).$ Eq. (3)

202

203 Total ^{210}Po fluxes at each depth, therefore, are the sum of the steady state values based only on

204 the ^{210}Po deficit (Eq. 2), $\lambda_{Po}(I_{Pb} - I_{Po})$, and vertical advective flux (Eq. 3), $w_{20} \times (A_{Po}^2 - A_{Po}^1)$.

205   The ECCO2 vertical velocities used in this study are the reanalysis products from the

206 Estimating the Circulation and Climate of the Ocean, Phase II (ECCO2) (Menemenlis et al.,

207 2008) project and the data were obtained from the Asia-Pacific Data-Research Center (APDRC,

208 http://apdrc.soest.hawaii.edu/las/v6/dataset?catitem=1). The ECCO2 model configuration uses a

209 cube-sphere grid projection with 18-km horizontal grid spacing and 50 vertical levels among

210 which there are 12 equal vertical layers from the surface to 120 m (Menemenlis et al., 2008). We

211 selected the ECCO2 grid points closest to the station and extracted vertical velocities from the

212 depths between z and $(z + 20 \text{ m})$ during 30 days prior to the sampling date at each station.

213 Because the deficit of ^{210}Po activity in the water column weighs the changes that occurred

214 shortly prior to the sampling time more heavily than those that occurred further back in time

215 (Verdeny et al., 2009), we chose to average the vertical velocity over one month rather than over

216 the mean life of ^{210}Po (200 days). The 30-day averaged vertical velocity was then used to

217 calculate vertical advective ^{210}Po export flux via Eq. (3) at each station.

218
219 **2.5. Satellite-based net primary production and phytoplankton composition**

220   The 8-day net primary production (NPP) data with a spatial resolution of 0.083º by 0.083º

221 were obtained from the Oregon State University Ocean Productivity standard products

222 (http://www.science.oregonstate.edu/ocean.productivity/), wherein NPP was estimated by the

223 Vertically Generalized Production Model (VGPM) (Behrenfeld and Falkowski, 1997). Due to

224 some missing data between November 2013 and February 2014, NPP for each station was

225 averaged for the previous 138 days (^{210}Po half-life) instead of 200 days (^{210}Po mean life).

226   Monthly average concentrations of diatoms, coccolithophores, cyanobacteria, chlorophytes,

227 and total chlorophyll with the spatial resolution of 0.67×1.25º were obtained from the Goddard

228 Earth Science Data and Information Services Center Interactive Online Visualization and

229 Analysis Infrastructure ("Giovanni") (https://giovanni.gsfc.nasa.gov/giovanni/, Acker and

230 Leptoukh, 2007). Time-series (October 2013 – July 2014, covering > 200 days before sampling)

231 data are averages over longitude for each month. We extracted data for the 5 basins individually

232 and calculated the fraction of each phytoplankton group at each station as the ratio of their

233 concentration to total chlorophyll concentration.

234

235 **3. Results**

236 **3.1. Satellite-derived seasonal NPP and phytoplankton composition**

237 The VGPM modeled NPP data along the GA01 transect was averaged over ~ 138 days (the

238 half-life of ^{210}Po) prior to the sampling date (see section 2.5, Table 1). Seasonal NPP at each

239 station varied from low values of 44 – 79 mmol C m^{-2} d^{-1} to a maximum value of 109 mmol C m$^-$

240 ^{2} d^{-1} at station 21. The Western European Basin had the highest seasonal NPP, followed by the

241 Iberian Basin; while the Iceland Basin, the Irminger Basin, and the Labrador Basin all had

242 similar NPP values in the range of 45 – 49 mmol C m^{-2} d^{-1}. There was a shift in the biological

243 community towards larger phytoplankton (e.g. diatoms) from east to west along the transect (Fig.

244 2). The basins where diatoms were the dominant phytoplankton group did not necessarily have

245 higher seasonal production relative to the basins where smaller phytoplankton (e.g.

246 coccolithophores) were more abundant. Indeed, the Iberian Basin had the second highest

247 seasonal NPP, despite the fact that the majority of chlorophyll was produced by coccolithophores.

248 Despite the evidence that earlier blooms may have been driven by diatoms (see section 4.2),

249 these observations highlight the possible contribution of small particles to production link

250 between small particles and production, and possibly to export (proportional to their role in

251 production according to Richardson and Jackson, 2007) along the transect. Moreover, this could

252 be also due to shorter blooms in the Irminger and Labrador Basins where the phytoplankton

253 growth was light-limited during winter compared to the condition in the Iberian and Western

254 European Basins.

255 The satellite-derived phytoplankton species composition demonstrated unique features within

256 the basins (Fig. 2). The Iberian Basin was dominated (> 60%) by coccolithophores between

257 October 2013 – July 2014, but had a gradual increase in the contribution of diatoms until April

258 2014 and a decreasing contribution after that. In the Western European Basin, station 26 was

259 dominated by diatoms all year around while station 21 was dominated by diatoms except in

260 October 2013 and July 2014 when the combination of chlorophytes and coccolithophores
261 contributed 35 – 77 % to ~~of~~ the total chlorophyll concentration. The stations in the Iceland,
262 Irminger, and Labrador Basins were all dominated (> 98%) by diatoms between October 2013
263 and July 2014. ~~during the 10-month time period.~~

264

265 **3.2. One-month averaged vertical velocity w_{20}**

266   The one-month averaged vertical velocities w_{20} ranged from -36 × 10^{-6} to 9 × 10^{-6} m s^{-1}
267 along the transect (negative: upwelling, positive: downwelling, Table 1). The standard deviations
268 of w_{20} were generally of the same order as the values of w_{20}. Particularly large standard
269 deviations, which exceed the typical values of the vertical velocity by a full order of magnitude,
270 were found at stations 13 (35-55 m, 110-130 m) and station 21 (110-130 m). These high standard
271 deviations suggest that the data of w_{20} should be used with great care. Downwelling was seen at
272 stations 38, 44, 64, and 77 with the velocities in the range of 1 to 9 × 10^{-6} m s^{-1}. Upwelling was
273 seen at the remaining stations, with highest intensity at station 60 near Greenland (absolute value:
274 11 – 36 × 10^{-6} m s^{-1}). The upwelling velocities were roughly equivalent at stations 1, 13, 21, 26,
275 32, and 69 (absolute value: 1 – 5 × 10^{-6} m s^{-1}).

276

277 **3.3. Total ^{210}Po deficits**

278   The vertical profiles of total ^{210}Po and ^{210}Pb activity at each station have been described in a
279 companion article (Tang et al., 2018). Here we show the section view of the ~~The~~ water column
280 ^{210}Po deficit (dpm 100 L^{-1}), which was calculated as total ^{210}Pb activity minus total ^{210}Po activity
281 (Fig. 3). There were small ^{210}Po deficits in the upper 100 m (including the majority of the depths
282 of MLD, $Z_{1\%}$, PPZ, and ThEq at all stations) at stations 1, 13, and 21, whereas a relatively large
283 excess of ^{210}Po was observed at 100 – 400 m depth. Station 60 had the highest deficits of ^{210}Po (~
284 8 dpm 100 L^{-1}, n = 5) at 40 – 120 m depth. A large surface deficit of ^{210}Po was found at station
285 64 (8 dpm 100 L^{-1}) and a surface excess was found at station 38 (-3.5 dpm 100 L^{-1}). There were
286 positive ^{210}Po deficits throughout most of the water column at stations in the Irminger and
287 Labrador Basins, whereas large ^{210}Po excesses (negative deficits) below 100 m were generally
288 seen in the Iberian Basin and Western European Basins. Such ^{210}Po excess was likely related to
289 the Iberian upwelling, which may have provided a source of ^{210}Po activity.

290

3.4. The ^{210}Po flux calculated from the deficit of ^{210}Po alone

Using the data of total ^{210}Po and ^{210}Pb activities, the amount of ^{210}Po escaping from the surface ocean via ~~activity~~ sinking ~~from the surface ocean via~~ particles ("^{210}Po fluxes", dpm m^{-2} d^{-1}) were calculated using Eq. (2) assuming steady state and ignoring advection and diffusion (Table 2, ^{210}Po/^{210}Pb term). The ^{210}Po fluxes were negligible or very low at stations 1, 21, and 38. At the other stations the ^{210}Po fluxes averaged 3.7 ± 1.4, 4.6 ± 2.6, 9.5 ± 4.9, and 14.4 ± 12 dpm m^{-2} d^{-1} at the MLD, $Z_{1\%}$, PPZ, and ThEq, respectively. The ^{210}Po fluxes tended to increase with depth at seven out of eleven stations (26, 38, 44, 60, 64, 69, and 77). At the MLD, $Z_{1\%}$ and PPZ, the largest ^{210}Po fluxes were all found in the Labrador Basin. The other 4 basins had relatively similar ^{210}Po export fluxes ($2.1 - 2.8$ dpm m^{-2} d^{-1}) at the MLD and $Z_{1\%}$. The West European Basin had much higher ^{210}Po flux (8.7 dpm m^{-2} d^{-1}) relative to that in the Iberian Basin (-0.1 dpm m^{-2} d^{-1}) at the PPZ. At the ThEq, on the other hand, the Irminger Sea had the highest ^{210}Po fluxes followed by the West European Basin. The lowest ^{210}Po fluxes at all investigated depths were generally found in the Iberian Basin.

3.5. POC/^{210}Po ratios in particles

Most of the ~~The~~ ratios of POC concentration to ^{210}Po activity (µmol dpm^{-1}) in the large size fraction (POC/^{210}Po_LSF, > 53 µm) were comparable to or higher than those ~~than~~ in the small size fraction (POC/^{210}Po_SSF, $1 - 53$ µm), whereas a few samples had values of POC/^{210}Po_LSF lower than those of POC/^{210}Po_SSF at stations 13, 26, 44, 64, and 77 ~~of particles by a factor of 2~~ (Table 3, Fig. 4a). The POC/^{210}Po ratio in the total particles (> 1 µm, the combination of small and large particles, POC/^{210}Po_TPF) was similar to that in the small particles (SSF), within about 97% (Table 3, Fig. 4b). This is because over 80% of the particulate ^{210}Po activity was associated with the small size fraction (Tang et al., 2018) likely due to the large surface area of abundant small particles. ~~Combined with~~ Because of the possible link between small particles and export along the transect discussed in section 3.1, and the results that scavenging of ^{210}Po was governed by the small particles (Tang et al., 2018), we propose to use ~~suggest that~~ this total particulate fraction along with the large size fraction ~~should be used~~ to ~~explain the water column ^{210}Po/^{210}Pb disequilibria and~~ calculate POC export along this cruise track.

The POC/^{210}Po in total particles (POC/^{210}Po_TPF) varied from 19 to 1300 ~~1400~~ µmol dpm^{-1} with a mean of 290 ± 320 µmol dpm^{-1} (n = 51, upper 800 m). The variability of POC/^{210}Po_TPF

ratios in this study is in line with previous observations in the Antarctic Circumpolar Current (300 - 1200 µmol dpm^{-1} for particles > 1 µm) (Friedrich and Rutgers van der Loeff, 2002), and the central Arctic (90 - 1900 µmol dpm^{-1} for particles > 53 µm) (Roca-Martí et al., 2016). The average ratio of 290 µmol dpm^{-1} is comparable to those observed in the central Equatorial Pacific (202 ± 90 µmol dpm^{-1} for particles > 0.45 µm) (Murray et al., 2005), the North Atlantic (290 ± 70 µmol dpm^{-1} for particles > 1 µm) (Rigaud et al., 2015), and the South Atlantic (113 ± 80 µmol dpm^{-1} for particles > 0.7 µm) (Sarin et al., 1999).

The measured POC/^{210}Po ratios in total particles at each station and depth were grouped into the 5 basins and fitted against depth using a single power law function in each basin (Fig. 5). The fit equations were used to calculate total particulate POC/^{210}Po ratios at the investigated depths at each station (Table 3).

4. Discussion

4.1. Physical advection effects on ^{210}Po export fluxes

In the study region, there were consistent patterns of circulation traveling through and near our sampling sites during the GEOVIDE cruise. From east to west the cruise track crossed the North Atlantic Current, the Eastern Reykjanes Ridge Current, the Irminger Current, the Irminger Gyre, the Western and Eastern Boundary Currents and the Labrador Current (Fig. 1 in García-Ibáñez et al., 2018). Additionally, short-lived eddies and fronts were also observed during the cruise, particularly in the OVIDE section from Portugal to Greenland (García-Ibáñez et al., 2018; Zunino et al., 2018). In this dynamic region advective influences may be important to include in calculations of ^{210}Po export. Despite this knowledge, we could not include horizontal advection in our model because the horizontal resolution of our sample sites was not sufficient to constrain reliable horizontal gradients of ^{210}Po activity in the study region. This assumption of negligible horizontal physical transport has been made in most ^{210}Po studies because of a similar lack of spatial resolution (e.g. Kim and Church, 2001; Stewart et al., 2010; Rigaud et al., 2015), and may be justified in some the open ocean settings where horizontal gradients in ^{210}Po activities are small (e.g. Wei et al., 2011). For more dynamic regimes such as along the GA01 transect, however, this assumption needs to be carefully evaluated, and the relative importance of advective ^{210}Po flux should be assessed if possible.

352 We did, however, have enough sampling depths at each station to assess the vertical

353 variability in ^{210}Po activity and to estimate the impact of vertical advection on the ^{210}Po flux ~~and~~

354 ~~distribution of radionuclide activities.~~ The range of ^{210}Po activity flux due to vertical advection (-

355 40 to 14 dpm m^{-2} d^{-1}, Table 2) was of the same magnitude as the steady state fluxes calculated

356 from the deficit alone (-5 to 37 dpm m^{-2} d^{-1}, Table 2). The magnitude of the uncertainty of the

357 ^{210}Po export flux due to vertical advection was influenced by the large variance in vertical

358 velocity field mentioned in Sect. 3.2. When excluding the three depths at stations 13 and 21

359 where the monthly vertical velocity average had substantial standard deviations (an order of

360 magnitude greater than w_{20}), the uncertainty of the ^{210}Po export flux was on average 2-fold

361 larger than the calculated ^{210}Po export flux. The largest positive vertical advective ^{210}Po fluxes

362 were at station 1 where the Iberian upwelling increased the calculated flux by 150 - 500%. The

363 largest negative vertical advective ^{210}Po fluxes were seen at station 60 where upwelling

364 decreased the ^{210}Po flux by 370 – 1100% at the depths of the MLD, ~~Z1%~~$Z_{1\%}$, and PPZ. This is

365 because the upwelling velocity was high at those depths (14 – 36 × 10^{-6} m s^{-1}, Table 1) and the

366 water upwelled was depleted in ^{210}Po activity. The vertical advective transport was smaller at the

367 MLD and $Z_{1\%}$ at station 13, at the ThEq at station 21, and at the PPZ and ThEq at station 64,

368 with the contributions lower than 6% to total ^{210}Po fluxes. Including vertical advection in our

369 flux estimates at all other depths, however, increased/decreased the ^{210}Po fluxes by 10 – 180%~~,~~

370 ~~and we must assume the horizontal advection could have influenced the ^{210}Po export flux at a~~

371 ~~similar scale~~. Like with vertical advection, neglecting horizontal advection can result in either an

372 underestimate or overestimate of ^{210}Po export flux depending on whether the advected water is

373 enriched or depleted in ^{210}Po. However, because our study region was characterized by distinct

374 water masses separated over 10s to 100s of meter in the vertical plane, whereas those same water

375 masses covered huge distances (100s to 1000s of kilometer) in the horizontal plane (Fig. 4 in

376 García-Ibáñez et al., 2018), vertical advection would most likely result in more change in

377 physical and chemical parameters over the scale of sampling than horizontal advection would.

378 Because the advective ^{210}Po export flux was calculated as the product of the velocity of the water

379 mass and the gradient of ^{210}Po activity in the corresponding direction, horizontal advection

380 would most likely contribute a much smaller range of advective ^{210}Po flux estimates.

381 Overall, the influence of physical advection on ^{210}Po activity may range from relatively

382 unimportant to dominant depending on study area. In this study, we observed physical processes

383 influencing ^{210}Po fluxes, in particular at stations 1 and 60. For future studies of ^{210}Po and ^{210}Pb

384 activity in regions of established upwelling or ocean margins, we suggest designing the sampling

385 plan so that the magnitude and variability of these processes may be incorporated into ^{210}Po

386 export models. At ocean margins, in particular, more water samples should be taken to improve

387 the resolution of horizontal features.

388

389 **4.2. Non-steady state effects on ^{210}Po export fluxes**

390 To our knowledge, three 3 systematic time-series studies of ^{210}Po and ^{210}Pb activities have

391 been conducted to date and have assessed, and the NSS effects on ^{210}Po fluxes have been

392 assessed. First, in the upper 500 m of the Sargasso Sea, Kim and Church, (2001) found that the

393 SS model may have overestimated and underestimated the ^{210}Po export fluxes in May and July

394 1997, respectively. Second, at At the DYFAMED site of the northwestern Mediterranean Sea,

395 the $\partial Po/\partial t$ term accounted for $\sim$ 50% of the observed ^{210}Po flux estimated by using the as

396 determined by SS model (Stewart et al., 2007). Last, in the South China Sea The the ^{210}Po export

397 fluxes at 1000 m calculated from the SS and NSS models in the South China Sea had similar

398 values within the uncertainties ((Wei et al., 2014). In fact, the SS model generally results in an

399 underestimation of the ^{210}Po flux under conditions of decreasing ^{210}Po activities in the water

400 column (i.e. when blooms switch from the productive phase to the export phase at certain stages

401 of the bloom events), whereas the SS model overestimates the flux for conditions of increasing

402 ^{210}Po activities (i.e. high atmospheric deposition).

403 Atmospheric aerosol deposition along the GA01 transect was reportedly low, without

404 significant influence of the Saharan plume (Shelley et al., 2017). The influence of atmospheric

405 deposition on the SS estimates obtained in this study, therefore, can be ignored. However, it is

406 important to assess the $\partial Po/\partial t$ term that was associated with the site-specific bloom events

407 during the cruise. Satellite estimates of net primary production (VGPM model) for the eight 8-

408 day periods ($\sim$ 2 months) prior to the sampling date ($\sim$ 2 months) were calculated at each station

409 (Fig. 67). Two months' NPP data is needed because such a time scale could ensure the sensitivity

410 for NSS estimates (Friedrich and Rutgers van der Loeff, 2002; Stewart et al., 2007). NPP for the

411 two-month period were in the ranges of 51 – 184, 39 – 403, 22 – 131, 18 – 204, 16 – 210 mmol

412 C m^{-2} d^{-1} in the Iberian Basin, the West European Basin, the Iceland Basin, the Irminger Basin,

14

413 and the Labrador Basin, respectively, indicating the occurrence of blooms during this time period

414 along the transect that might have influenced the ^{210}Po fluxes derived from Eq. (1).

415 ~~In general, time-series NPP data indicated that significant bloom events may have occurred~~

416 ~~prior to the sampling date at most of the stations, thus~~ Assuming ~~assuming~~ SS may have

417 underestimated the ^{210}Po export along the GA01 transect depending on the stage of the bloom

418 before sampling. For example, at station 21 the largest NPP peak (403 mmol C m^{-2} d^{-1}) occurred

419 2 weeks before our sampling date and diminished rapidly ($\sim$ 100 mmol C m^{-2} d^{-1} at sampling

420 time). The combination of ~~very~~ high phytoplankton export and sudden decrease in NPP may

421 have significantly lowered the ^{210}Po activity in the upper waters, resulting in a negative $\partial Po/\partial t$,

422 and thus the SS model may have underestimated the true ^{210}Po flux. Temporal variations were

423 also seen in the time-series phytoplankton community composition, in particular at stations 1 and

424 13 (Fig. 2). Both stations were dominated ($> 60\%$) by coccolithophores between October 2013 –

425 July 2014, but appeared to have a diatom bloom in April 2014 before sampling. Polonium-210

426 and ^{210}Pb tend to bind to specific biopolymeric functional groups, leading to fractionation during

427 their sorption onto particles (Quigley et al., 2002; Chuang et al., 2013; Yang et al., 2013). The

428 temporal variation of phytoplankton composition could therefore also lead to non-steady state

429 effects on the overall ^{210}Po activity balance, which are difficult to assess but deserve more

430 attention.

431 The NSS effect on the ^{234}Th fluxes at the ThEq were evaluated during the same cruise along

432 the GA01 transect in Lemaitre et al., (2018) by using the NSS model developed in Savoye et al.,

433 (2006). Because the cruise plan did not allow an opportunity to reoccupy the study areas over

434 time, the authors made the assumption that ^{234}Th activity was in equilibrium with ^{238}U activity at

435 the starting date of the bloom. Their results suggested that the NSS ^{234}Th fluxes were about 1.1

436 to 1.3 times ~~fold~~ higher than the SS estimates in the Iberian and West European Basins, and 1.4

437 to 2.1 times ~~2-fold~~ higher in the Iceland, Irminger, and the Labrador Basins. We did not attempt

438 to apply the same technique to estimate NSS ^{210}Po fluxes in this study because the assumption of

439 equilibrium between ^{210}Po activity and ^{210}Pb activity at the starting date of the bloom may be

440 inappropriate since~~. One confounding factor is the timescale of events;~~ the ^{210}Po deficit integrates

441 over a longer time period (months) than a typical bloom event (days/weeks).

442

443 **4.3. POC flux calculated from ^{210}Po flux**

The POC export fluxes were calculated by multiplying both the [210]Po export fluxes calculated from the deficit alone (SS without advection) and the total [210]Po fluxes (sum of the fluxes calculated from the [210]Po deficit and vertical advection)~~combined [210]Po fluxes of the deficit-based fluxes and the vertical advective term with~~ by the total particulate (> 1 μm) POC/[210]Po ratios at the corresponding depths (Table 2, Fig. 6̶7). The POC fluxes calculated from only the deficit term and the total term ranged from negligible to 7 mmol C m^{-2} d^{-1} and from negative to 10 mmol C m^{-2} d^{-1}, respectively. This is in good agreement with the SS fluxes derived via the [210]Po/^{210}Pb method ignoring advection in other regions of the world ocean (negligible to 8.5 mmol C m^{-2} d^{-1}) (e.g. Shimmield et al., 1995; Sarin et al., 1999; Kim and Church, 2001; Stewart et al., 2007; Verdeny et al., 2008; Roca-Martí et al., 2016; Subha Anand et al., 2017).

The highest estimated POC fluxes (Table 2) along the transect were observed at most of the investigated depths in the Labrador Sea and at the Greenland Shelf, whereas the lowest export was in the Iberian and West European Basins. An exception to this pattern was found at station 26 where POC flux was actually similar in magnitude to the flux at stations 64 and 69. Station 26 was located in the middle of the Subarctic Front (SAF), a cold and fresh anomaly originating from subpolar water (Zunino et al., 2018). The hydrographic properties associated with the SAF appear to promote high primary production (174 ± 19 6̶ mmol C m^{-2} d^{-1}, Table 1) and subsequently high carbon export (Kemp et al., 2006; Rivière and Pondaven, 2006; Guidi et al., 2007; Waite et al., 2016). While stations ~~Stations~~ on the Greenland Shelf (stations 60 and 64) had the greatest estimated carbon export at the depth of ThEq (5 – 10 mmol C m^{-2} d^{-1}), station 60 at the depth of $Z_{1\%}$ had the lowest POC flux (-12.5 to -8.4 mmol C m^{-2} d^{-1}).

The negligible deficit of [210]Po at the MLD and $Z_{1\%}$ seen at stations 21, 38 and 44 leads to negligible [210]Po-derived POC fluxes at those depths and stations (Table 2, Fig. 6̶7). The relatively low POC export (negligible – 1.7 mmol C m^{-2} d^{-1}) at stations 1 and 13, on the other hand, resulted from low particulate POC/[210]Po ratios (Table 2). In fact, the Iberian Basin had the lowest measurements of particulate POC/[210]Po ratios in both the small and large size fractions relative to the other four basins along the transect (Fig. 4). This basin was also the only region along the transect where the phytoplankton community was not dominated by diatoms but by smaller phytoplankton, in particular coccolithophores. Smaller phytoplankton cells could

474   scavenge more ^{210}Po (higher particulate ^{210}Po activity relative to the large particles) due to larger

475   surface area per unit of volume, lowering their ratio of POC concentration to ^{210}Po activity.

476

477   **4.4. POC export efficiency**

478   The POC export flux calculated from the total ^{210}Po flux at the depth of the PPZ was

479   compared to the satellite-derived NPP over ~ 138 days (see section 2.5) at each station, and the

480   ratio was reported as the POC export efficiency.

481   The export efficiencies in this study were below 10% at 10 out of 11 stations, averaging 6 ± 4%

482   (n = 10, excluding the negative value at station 60, Fig. 8). Export efficiencies < 10% observed

483   here were similar to those found in the Equatorial Pacific, the Arabian Sea, and at the BATS site

484   (Buesseler, 1998; Subha Anand et al., 2017), but lower than those reported at high latitude sites

485   (> 25%) such as the Arctic (Gustafsson and Andersson, 2012; Moran et al., 1997; Roca-Martí et

486   al., 2016), the Bellingshausen Sea (Shimmield et al., 1995), and the Antarctic Polar Front

487   (Rutgers van der Loeff et al., 1997).

488   Export efficiencies ranged from 0.5 to 2.5% in the Iberian Basin ~~(1 ± 1%)~~, while the values

489   in the Irminger Basin (3 ± 3%, excluding station 60) were similar to the export efficiencies in the

490   Western European Basin (5 ± 5%) and in the Iceland Basin (6 ± 6%). The export efficiencies, in

491   contrast, were ~~significantly~~ larger in the Labrador Basin (10 ± 3%). The lowest export

492   efficiencies observed in the Iberian Basin were consistent with the dominance of smaller

493   phytoplankton species there (coccolithophores and cyanobacteria; Fig. 2). Indeed, small cells are

494   usually slow-sinking particles that are likely more prone to degradation (Villa-Alfageme et al.,

495   2016), leading to lower export efficiencies. Conversely, the higher export efficiencies at other

496   stations, all generally dominated by diatoms (Fig. 2), support the idea that diatoms may be more

497   efficient in exporting POC than smaller phytoplankton (Buesseler, 1998). Differences in export

498   efficiencies between the basins dominated by diatoms suggest that other factors may also play

499   some role (e.g., temporal decoupling between production and export). ~~This trend was consistent~~

500   ~~with the changes that occurred in the phytoplankton community composition along the transect.~~

501   ~~In particular, the basins where diatoms dominated the phytoplankton community generally had~~

502   ~~higher export efficiencies relative to the export efficiencies in the Iberian Basin where smaller~~

503   ~~phytoplankton, like coccolithophores, were more abundant (Fig. 2), supporting diatoms'~~

504 ~~significant role in efficiently driving local POC export and smaller phytoplankton, may not be as~~

505 ~~efficient as diatoms in compelling export production (e.g. Murray et al., 1996; Buesseler, 1998).~~

506 The POC export efficiency could also vary widely within the same basin~~, particularly within~~

507 ~~the Iberian and Western European Basins~~. Taking the two stations in the West~~ern~~ European

508 Basin for instance, export efficiency at station 26 was ~ 5-fold greater than that estimated at

509 station 21, likely consistent with a lower contribution of diatoms and a higher contribution of

510 smaller phytoplankton at station 21 relative to those at station 26 (Fig. 2).~~ Even though~~ But

511 overall the time-series composition of the phytoplankton community at the two stations was ~~very~~

512 similar (Fig. 2)~~, the efficiency of carbon export differed~~. The site-specific environment may have

513 impacted the export of the same cell type to different degrees (Durkin et al., 2016). Station 26

514 was in the middle of the SAF, and the mesoscale physical processes (i.e. turbulence and mixing)

515 at the front can introduce nutrients into the local euphotic zone (Lévy et al., 2012). Large

516 phytoplankton species generally dominate in these nutrients-rich waters and can promote

517 massive episodic particle export (e.g. Kemp et al., 2006; Guidi et al., 2007; Waite et al., 2016).

518

519 **4.5. Comparison of ^{210}Po and ^{234}Th derived POC fluxes**

520 The measurements of ^{234}Th/^{238}U disequilibrium to estimate POC export flux were

521 simultaneously carried out during the GEOVIDE cruise (Lemaitre et al., 2018). The authors

522 discussed the influence of vertical advection on ^{234}Th export flux and conclude it can be

523 neglected. In the present study, ~~The~~ estimates of ^{234}Th-derived POC (^{234}Th-POC) flux were

524 compared to ^{210}Po-derived POC (^{210}Po-POC) flux. To avoid discrepancies, both the ^{234}Th-POC

525 and ^{210}Po-POC flux estimates were calculated at the depth of ThEq using the POC/radionuclide

526 ratio in total particles > 1 μm (TPF) and large particles > 53 μm (LSF), and both methods

527 ignored physical transport and assumed steady state, where any deviation from secular

528 equilibrium was created by sinking particles with an adsorbed and/or absorbed excess of the

529 short-lived daughter isotope.

530

531 **4.5.1. ^{210}Po flux vs. ^{234}Th flux**

532 The integrated ^{210}Po and ^{234}Th flux~~es~~ at ~~over~~ the depth of ThEq were compared (Fig. 9).

533 There was a spatial trend of ^{234}Th flux, but not ^{210}Po flux along the transect; ^{234}Th fluxes at

534 stations 1 to 38 (eastern section, 1580 ± 430 dpm m^{-2} d^{-1}) were significantly greater (Wilcoxon

535 rank sum test, p-value < 0.002) than the fluxes at stations 44 to 77 (western section, 710 ± 230

536 dpm m^{-2} d^{-1}). The means of the ^{210}Po fluxes in the western and eastern sections were not

537 statistically different from each other (Wilcoxon rank sum test, p-value = 0.3). However, the flux

538 of ^{210}Po and ^{234}Th correlated with each other better in the western (n = 5, R^2 = 0.6) than in the

539 eastern (n = 6, R^2 = 0.01) sections.

540 These relationships may be related to both the stage of the bloom and different half-lives of

541 the two isotopes. Indeed, ^{234}Th fluxes integrate the conditions that occurred days to weeks prior

542 to the sampling date while the ^{210}Po method integrates the flux over the past few months. Within

543 the Iberian Basin, stations 1 and 13 were sampled weeks to months after the bloom development

544 (Fig. 6). The moderate to relatively high ^{234}Th fluxes are thus surprising. ~~Most stations in the~~

545 ~~western section were sampled at the time when the spring bloom was declining (Fig. 7). In~~

546 ~~contrast, the sampling in the eastern section was conducted weeks to months after the bloom.~~ in

547 ~~the Iberian Basin and during the bloom in the West European and Iceland Basins.~~ Lemaitre et al.,

548 (2018) argue that the greater fluxes there might be related to the proximity of the Iberian margin,

549 where particle dynamics were intense and lithogenic particles were numerous (Gourain et al.,

550 2018). A temporal decoupling between production and export can be an alternative possibility.

551 The Western European and Icelandic Basins were sampled during bloom development, and the

552 NPP peaks occuring just before sampling may have promoted the high fluxes. In fact, these

553 basins have been characterized by the presence of fast-sinking particles during the bloom (Villa-

554 Alfageme et al., 2016), likely also explaining the high exports. In contrast, the lower exprot

555 observed in the western section may be due to the fact that the sampling occurred during the

556 decline of the bloom, probabaly with a decoupling between production and export in the

557 Labrador Basin, or during particle retention event in the Irminger Basin.

558 Unlike the observation of higher ^{234}Th export flux in the eastern than western sections, there

559 was no significant difference in ^{210}Po export flux between the two sections. This observation

560 supports the argument that the ^{210}Po deficit tends to smooth out episodic events due to

561 integration over longer time periods. The ^{210}Po deficit records seasonal changes in export fluxes,

562 whereas the ^{234}Th deficit represents more recent changes in the water column (Verdeny et al.,

563 2009; Hayes et al., 2018). Indeed, the ^{210}Po deficit integrates the flux over months that include a

564 period of lower flux prior to the bloom along the GA01 transect, whereas the ^{234}Th deficit

565 integrates the flux only over weeks that include the bloom itself at most of the stations (Fig. 6).

566 Therefore, the specific stage of the bloom shortly prior to the sampling date appears to have less

567 influence on the ^{210}Po-derived than the ^{234}Th-derived export flux along this transect. ~~Thorium-~~

568 ~~234 fluxes integrate the conditions that occurred days to weeks prior to the sampling date while~~

569 ~~the ^{210}Po method integrates the flux over the past few months. In the eastern section, the sinking~~

570 ~~flux of ^{234}Th seemed to reflect the recent or current high export events, but longer integration via~~

571 ~~the ^{210}Po/^{210}Pb method tended to reduce the impact of such events, resulting in large~~

572 ~~discrepancies between ^{234}Th and ^{210}Po fluxes. In the western section, on the other hand, the~~

573 ~~spatial trend of the ^{234}Th and ^{210}Po export fluxes were more consistent with each other when the~~

574 ~~export of radionuclides was assessed just after the bloom.~~

575

576 ### 4.5.2. POC/^{210}Po vs. POC/^{234}Th ratio

577 In order to calculate POC export flux, one needs both the export of the daughter nuclide at a

578 defined depth as well as the particulate POC/radionuclide ~~^{210}Po~~ ratio on the sinking particles. In

579 situ pump filtered particles, either operationally defined as small (1-53 μm, SSF), large (> 53 μm,

580 LSF), or total (> 1 μm, TPF) particles, may all represent a combination of sinking and non-

581 sinking particles. In the present study, the particulate POC/radionuclide ratio on the TPF and

582 LSF were examined and used to calculate POC export flux. The POC/^{210}Po and POC/^{234}Th ratios

583 in the particles ~~> 1 μm~~ of TPF and LSF at the depths of ThEq were derived from the power law

584 functions in each basin (POC/^{210}Po in Table 2, POC/^{234}Th in Lemaitre et al., (2018)~~not shown~~).

585 The TPF POC/^{210}Po and TPF POC/^{234}Th ratios had very similar spatial trends (n = 11, R^2 = 0.8,

586 p-value < 0.0001) along the transect, with the lowest POC/radionuclide ratios in the Iberian and

587 Western European Basins and the highest ratios in the Labrador Sea ~~and moderate ratios in~~

588 ~~between~~. In contrast, the LSF POC/^{210}Po ratios were not correlated with LSF POC/^{234}Th ratios (n

589 = 11, R^2 = 0.3, p-value =0.07). The correlation of values within the TPF but not the LSF suggests

590 that the composition of large particles was different from that of the total particles, and that the

591 difference in particle association between POC and ^{210}Po and ^{234}Th was greater in large than total

592 particles.

593

594 ### 4.5.3. ^{210}Po-derived POC vs. ^{234}Th-derived POC

595 When the radionuclide fluxes were multiplied by the POC/radionuclide values, the range of

596 the calculated POC fluxes were ~~from~~ negligible to 7 mmol C m^{-2} d^{-1} and negligible to 12 mmol C

597   m^{-2} d^{-1} via the ^{210}Po method using the TPF and LSF POC/^{210}Po ratios, respectively; and from 2.5

598   to 13 mmol C m^{-2} d^{-1} and from 1 to 12 mmol C m^{-2} d^{-1} via the ^{234}Th method using the TPF and

599   LSF POC/^{234}Th ratios, respectively (Fig. 10). The ^{234}Th-POC and ^{210}Po-POC fluxes agreed

600   within a factor of 3 along the transect, with higher POC estimates derived from the ^{234}Th method

601   in 9 out of 11 stations. This was consistent with previous studies that have typically found higher

602   estimated POC flux via the ^{234}Th method (e.g. Shimmield et al., 1995; Stewart et al., 2007;

603   Verdeny et al., 2009).

604   When using the total particle POC/radionuclide ratios, only ~~Only at~~ stations 26 and 60 were

605   ~~there~~ characterized by slightly higher ^{210}Po-derived POC flux estimates than ^{234}Th-derived

606   estimates (0.2 and 1.5-fold, respectively~~< 1-fold~~). In contrast, at station 1 the difference between

607   the methods was ~~the~~ greatest, with the ^{210}Po-derived POC flux negligible and the ^{234}Th-POC flux

608   of about 7 mmol C m^{-2} d^{-1}. At stations 13, 21, and 44, the ^{234}Th-POC fluxes were greater than

609   ^{210}Po-POC estimates by almost 1-fold. Whereas in the Iceland and Labrador Basins, the ^{234}Th-

610   POC fluxes were larger than ^{210}Po-POC estimates by 3- and 2-fold, respectively. When using the

611   large particle POC/radionuclide ratios, only in the Irminger Basin was there higher ^{210}Po-derived

612   POC flux than ^{234}Th-derived POC flux (> 0.2 to 3-fold). In the Iberian Basin, the greatest

613   difference between the methods was found at station 1 where ^{210}Po-derived POC flux was

614   negligible while ^{234}Th-derived POC flux was the highest along the transect but with a large

615   uncertainty (12 ± 22 mmol C m^{-2} d^{-1}), and at station 13 the ^{234}Th-POC flux was greater than the

616   ^{210}Po-POC estimate by 4-fold. In the Western European, Iceland, and Labrador Basins, the ^{234}Th-

617   POC fluxes were larger than ^{210}Po-POC estimates by 5, 4, and 2-fold, respectively.

618   Wilcoxon rank sum tests revealed that the ^{234}Th-POC estimates were significantly greater

619   than ^{210}Po-derived POC export at the stations from the Iberian Basin to the Iceland Basin (n = 6,

620   TPF: p-value < 0.01, LSF: p-value < 0.02), but not at the stations from the Irminger Basin to the

621   Labrador Basin (n = 5, TPF: p-value > 0.1, LSF: p-value = 1). Since the ratios of POC to

622   radionuclides on total particles ~~POC/^{234}Th and POC/^{210}Po ratios~~ had very similar spatial trends

623   along the transect, the discrepancy between TPF ^{234}Th-POC and TPF ^{210}Po-POC flux estimates

624   ~~seems to~~ must be driven primarily by the discrepancy between the SS estimates of ^{234}Th and

625   ^{210}Po fluxes, discussed in section 4.5.1. In contrast, the discrepancy between the POC to isotope

626   ratios in the large particle may have led to some degree of discrepancy between the LSF ^{234}Th-

627   POC and LSF ^{210}Po-POC flux estimates.

5. Conclusions

This study used the water column ^{210}Po and ^{210}Pb activity data to constrain the ^{210}Po particulate flux from the mixed layer depth, the base of the euphotic zone and primary production zone, and the ^{234}Th-^{238}U equilibrium depth MLD, the base of $Z_{1\%}$ and PPZ, and the depth of THEq. The ratio of POC concentration to ^{210}Po activity on the total particulate (> 1 μm) fraction was used to estimate POC export fluxes. We have been able to include vertical advection into a steady-state model to calculate the ^{210}Po flux along the transect. The scale of ^{210}Po fluxes due to vertical advection were of the same magnitude as the steady state fluxes calculated from the ^{210}Po deficit alone. The ^{210}Po-derived POC export fluxes varied spatially, ranging from negligible to 10 mmol C m^{-2} d^{-1} along the transect, with the highest export fluxes in the Labrador Sea. POC export efficiencies (flux relative to production) also showed regional differences, ranging from negligible to 13% along the transect. Higher export efficiencies were seen in the basins where diatoms dominated the phytoplankton community. The low export efficiencies recorded in the Iberian Basin, on the other hand, may be associated with the dominance of smaller phytoplankton, such as coccolithophores. POC export fluxes estimated from the water column ^{210}Po/^{210}Pb and ^{234}Th/^{238}U disequilibria agreed within a factor of 3 across our study region, with higher POC estimates generally derived from the ^{234}Th method. The differences were attributed to integration timescales and the history of bloom events.

671 **References**

672 Acker, J. G. and Leptoukh, G.: Online Analysis Enhances Use of NASA Earth Science Data, Eos,
673 Trans. AGU, 88, 14-17, 2007.
674
675 Bhat, S. G., Krishnaswamy, S., Lal, D., Rama and Moore, W. S.: 234Th/238U ratios in the ocean,
676 Earth and Planetary Science Letters, 5 IS -, 483-491, 1968.
677
678 Buesseler, K. O.: The decoupling of production and particulate export in the surface ocean,
679 Global Biogeochemcal Cycles, 12, 297-310, 10.1029/97GB03366, 1998.
680
681 Buesseler, K. O., Bacon, M. P., Kirk Cochran, J. and Livingston, H. D.: Carbon and nitrogen
682 export during the JGOFS North Atlantic Bloom experiment estimated from 234Th:238U
683 disequilibria, Deep Sea Research Part A. Oceanographic Research Papers, 39, 1115-1137, 1992.
684
685 Cherrier, J., Burnett, W. C. and LaRock, P. A.: Uptake of polonium and sulfur by bacteria,
686 Geomicrobiology Journal, 13, 103-115, 10.1080/01490459509378009, 1995.
687
688 Chuang, C., Santschi, P. H., Ho, Y., Conte, M. H., Guo, L., Schumann, D., Ayranov, M. and Li,
689 Y.: Role of biopolymers as major carrier phases of Th, Pa, Pb, Po, and Be radionuclides in
690 settling particles from the Atlantic Ocean, Marine Chemistry, 157, 131-143, 2013.
691
692 Cochran, J. K.: Uranium-Series Disequilibrium - Application to Earth, Marine, and
693 Environmental Sciences, The oceanic chemistry of the uranium and thorium-series nuclides.
694 Oxford University Press, 334-395, 1992.
695
696 Djogic, R., Sipos, L. and Branica, M.: Characterization of uranium(VI) in seawater, Limnology
697 and Oceanography, 31, 1122-1131, 10.4319/lo.1986.31.5.1122, 1986.
698
699 Ducklow, H., Steinberg, D. and Buesseler, K.: Upper Ocean Carbon Export and the Biological
700 Pump, Oceanography, 14, 50-58, 10.5670/oceanog.2001.06, 2001.
701
702 Durkin, C. A., Van Mooy, B. A. S., Dyhrman, S. T. and Buesseler, K. O.: Sinking phytoplankton
703 associated with carbon flux in the Atlantic Ocean, Limnology and Oceanography, 61, 1172-1187,
704 10.1002/lno.10253, 2016.
705
706 Falkowski, P. G., Barber, R. T. and Smetacek, V.: Biogeochemical Controls and Feedbacks on
707 Ocean Primary Production, Science, 281, 200-206, 1998.
708
709 Fisher, N. S., Burns, K. A., Cherry, R. D. and Heyraud, M.: Accumulation and cellular
710 distribution of 241Am, 210Po and 210Pb in two marine algae, Marine Ecology Progress Series,
711 11, 233-237, 1983.
712
713 Fleer, A. P. and Bacon, M. P.: Determination of 210Pb and 210Po in seawater and marine
714 particulate matter, Nuclear Instruments and Methods in Physics Research, 223, 243-249, 1984.
715

716   Flynn, W. W.: The determination of low levels of polonium-210 in environmental materials,
717   Analytica Chimica Acta, 43, 221-227, 1968.
718
719   Fonseca-Batista, D., Li, X., Riou, V., Michotey, V., Fripiat, F., Deman, F., Guasco, S., Brion, N.,
720   Lemaitre, N., Planchon, F., Tonnard, M., Planquette, H., Gallinari, M., Sarthou, G., Elskens, M.,
721   Chou, L. and Dehairs, F.: Evidence of high N2 fixation rates in productive waters of the
722   temperate Northeast Atlantic, Biogeosciences, 2018.
723
724   Friedrich, J. and Rutgers van der Loeff, M. M.: A two-tracer (210Po–234Th) approach to
725   distinguish organic carbon and biogenic silica export flux in the Antarctic Circumpolar Current,
726   Deep Sea Research Part I: Oceanographic Research Papers, 49, 101-120, 10.1016/S0967-
727   0637(01)00045-0, 2002.
728
729   García-Ibáñez, M. I., Pérez, F. F., Lherminier, P., Zunino, P., Mercier, H. and Tréguer, P.: Water
730   mass distributions and transports for the 2014 GEOVIDE cruise in the North Atlantic,
731   Biogeosciences, 15, 2075-2090, https://doi.org/10.5194/bg-15-2075-2018, 2018.
732
733   Gourain, A., Planquette, H., Cheize, M., Menzel-Barraqueta, J. L., Boutorh, J., Shelley, R. U.,
734   Pereira-Contreira, L., Lemaitre, N., Lacan, F., Lherminier, P. and Sarthou, G.: Particualte trace
735   metals along the GEOVIDE section, Biogeosciences, 2018.
736
737   Guidi, L., Stemmann, L., Legendre, L., Picheral, M., Prieur, L. and Gorsky, G.: Vertical
738   distribution of aggregates (>110 µm) and mesoscale activity in the northeastern Atlantic: Effects
739   on the deep vertical export of surface carbon, Limnology and Oceanography, 52, 7-18,
740   doi:10.4319/lo.2007.52.1.0007, 2007.
741
742   Hayes, C. T., Black, E. E., Anderson, R. F., Baskaran, M., Buesseler, K. O., Charette, M. A.,
743   Cheng, H., Cochran, J. K., Edwards, R. L., Fitzgerald, P., Lam, P. J., Lu, Y., Morris, S. O.,
744   Ohnemus, D. C., Pavia, F. J., Stewart, G. and Tang, Y.: Flux of Particulate Elements in the North
745   Atlantic Ocean Constrained by Multiple Radionuclides, Global Biogeochemical Cycles, 32,
746   doi:10.1029/2018GB005994, 2018.
747
748   Honjo, S., Manganini, S. J., Krishfield, R. A. and Francois, R.: Particulate organic carbon fluxes
749   to the ocean interior and factors controlling the biological pump: A synthesis of global sediment
750   trap programs since 1983, Progress in Oceanography, 76, 217-285, 2008.
751
752   Jerlov, N. G.: Optical Oceanography. Elsevier Publishing Company, 1968.
753
754   Kemp, A. E. S., Pearce, R. B., Grigorov, I., Rance, J., Lange, C. B., Quilty, P. and Salter, I.:
755   Production of giant marine diatoms and their export at oceanic frontal zones: Implications for Si
756   and C flux from stratified oceans, Global Biogeochemical Cycles, 20,
757   doi:10.1029/2006GB002698, 2006.
758
759   Kim, G. and Church, T. M.: Seasonal biogeochemical fluxes of 234Th and 210Po in the Upper
760   Sargasso Sea: Influence from atmospheric iron deposition, Global Biogeochemcal Cycles, 15,
761   651-661, 10.1029/2000GB001313, 2001.

25

Lemaitre, N., Planchon, F., Planquette, H., Dehairs, F., Batista, D. F., Roukaerts, A., Deman, F., Tang, Y., Mariez, C. and Sarthou, G.: High variability of export fluxes along the North Atlantic GEOTRACES section GA01: Particulate organic carbon export deduced from the 234Th method, Biogeosciences, 15, 6417-6437, https://doi.org/10.5194/bg-15-6417-2018, 2018.

Lévy, M., Iovino, D., Resplandy, L., Klein, P., Madec, G., Tréguier, A. M., Masson, S. and Takahashi, K.: Large-scale impacts of submesoscale dynamics on phytoplankton: Local and remote effects, Ocean Modelling, 43-44, 77-93, https://doi.org/10.1016/j.ocemod.2011.12.003, 2012.

Masqué, P., Sanchez-Cabeza, J. A., Bruach, J. M., Palacios, E. and Canals, M.: Balance and residence times of 210Pb and 210Po in surface waters of the northwestern Mediterranean Sea, Continental Shelf Research, 22, 2127-2146, 10.1016/S0278-4343(02)00074-2, 2002.

Menemenlis, D., Campin, J., Heimbach, P., Hill, C., Lee, T., Nguyen, A., Schodlock, M. and Zhang, H.: ECCO2: High Resolution Global Ocean and Sea Ice Data Synthesis, Mercator Ocean Quarterly Newsletter, 31, 13-21, 2008.

Moore, H. E., Poet, S. E., Martell, E. A. and Wilkening, M. H.: Origin of 222Rn and its long lived daughters in air over Hawaii, Journal of Geophysical Research, 79, 5019-5024, doi:10.1029/JC079i033p05019, 1974.

Murray, J. W., Paul, B., Dunne, J. P. and Chapin, T.: 234Th, 210Pb, 210Po and stable Pb in the central equatorial Pacific: Tracers for particle cycling, Deep Sea Research Part I: Oceanographic Research Papers, 52, 2109-2139, 2005.

Murray, J. W., Young, J., Newton, J., Dunne, J., Chapin, T., Paul, B. and McCarthy, J. J.: Export flux of particulate organic carbon from the central equatorial Pacific determined using a combined drifting trap-234Th approach, Deep Sea Research Part II, 43, 1095-1132, 10.1016/0967-0645(96)00036-7, 1996.

Owens, S. A., Pike, S. and Buesseler, K. O.: Thorium-234 as a tracer of particle dynamics and upper ocean export in the Atlantic Ocean, Deep Sea Research Part II, 116, 42-59, 10.1016/j.dsr2.2014.11.010, 2015.

Quigley, M. S., Santschi, P. H., Hung, C., Guo, L. and Honeyman, B. D.: Importance of acid polysaccharides for 234Th complexation to marine organic matter, Limnology and Oceanography, 47, 367-377, 10.4319/lo.2002.47.2.0367, 2002.

Richardson, T. L. and Jackson, G. A.: Small Phytoplankton and Carbon Export from the Surface Ocean, Science, 315, 838-840, 10.1126/science.1133471, 2007.

Rigaud, S., Puigcorbé, V., Camara-Mor, P., Casacuberta, N., Roca-Martí, M., Garcia-Orellana, J., Benitez-Nelson, C. R., Masqué, P. and Church, T.: A methods assessment and recommendations for improving calculations and reducing uncertainties in the determination of 210Po and 210Pb

808 activities in seawater, Limnology and Oceanography Methods, 11, 561-571,
809 10.4319/lom.2013.11.561, 2013.
810
811 Rigaud, S., Stewart, G., Baskaran, M., Marsan, D. and Church, T.: 210Po and 210Pb distribution,
812 dissolved-particulate exchange rates, and particulate export along the North Atlantic US
813 GEOTRACES GA03 section, Deep Sea Research Part II, 116, 60-78,
814 10.1016/j.dsr2.2014.11.003, 2015.
815
816 Rivière, P. and Pondaven, P.: Phytoplankton size classes competitions at sub-mesoscale in a
817 frontal oceanic region, Journal of Marine Systems, 60, 345-364,
818 https://doi.org/10.1016/j.jmarsys.2006.02.005, 2006.
819
820 Roca-Martí, M., Puigcorbé, V., Rutgers van der Loeff, M. M., Katlein, C., Fernández-Méndez,
821 M., Peeken, I. and Masqué, P.: Carbon export fluxes and export efficiency in the central Arctic
822 during the record sea-ice minimum in 2012: a joint 234Th/238U and 210Po/210Pb study, Journal
823 of Geophysical Research: Oceans, 121, 5030-5049, 10.1002/2016JC011816, 2016.
824
825 Rutgers van der Loeff, M. M., Friedrich, J. and Bathmann, U. V.: Carbon export during the
826 Spring Bloom at the Antarctic Polar Front, determined with the natural tracer 234Th, Deep Sea
827 Research Part II, 44, 457-478, 10.1016/S0967-0645(96)00067-7, 1997.
828
829 Sabine, C. L.: The Oceanic Sink for Anthropogenic CO2, Science, 305, 367-371,
830 10.1126/science.1097403, 2004.
831
832 Sarin, M. M., Kim, G. and Church, T. M.: 210Po and 210Pb in the South-equatorial Atlantic:
833 distribution and disequilibrium in the upper 500 m, Deep Sea Research Part II, 46, 907-917,
834 1999.
835
836 Savoye, N., Benitez-Nelson, C., Burd, A. B., Cochran, J. K., Charette, M., Buesseler, K. O.,
837 Jackson, G. A., Roy-Barman, M., Schmidt, S. and Elskens, M.: 234Th sorption and export
838 models in the water column: A review, Marine Chemistry, 100, 234-249, 2006.
839
840 Shelley, R. U., Roca-Martí, M., Castrillejo, M., Sanial, V., Masqué, P., Landing, W. M., van
841 Beek, P., Planquette, H. and Sarthou, G.: Quantification of trace element atmospheric deposition
842 fluxes to the Atlantic Ocean (> 40°N; GEOVIDE, GEOTRACES GA01) during spring 2014,
843 Deep Sea Research Part I: Oceanographic Research Papers, 119, 34-49,
844 10.1016/j.dsr.2016.11.010, 2017.
845
846 Shimmield, G. B., Ritchie, G. D. and Fileman, T. W.: The impact of marginal ice zone processes
847 on the distribution of 210Pb, 210Po and 234Th and implications for new production in the
848 Bellingshausen Sea, Antarctica, Deep Sea Research Part II, 42, 1313-1335, 10.1016/0967-
849 0645(95)00071-W, 1995.
850
851 Stewart, G., Cochran, J. K., Miquel, J. C., Masqué, P., Szlosek, J., Rodriguez y Baena, A. M.,
852 Fowler, S. W., Gasser, B. and Hirschberg, D. J.: Comparing POC export from 234Th/238U and
853 210Po/210Pb disequilibria with estimates from sediment traps in the northwest Mediterranean,

854   Deep Sea Research Part I: Oceanographic Research Papers, 54, 1549-1570,
855   10.1016/j.dsr.2007.06.005, 2007.

857   Stewart, G. M., Bradley Moran, S. and Lomas, M. W.: Seasonal POC fluxes at BATS estimated
858   from 210Po deficits, Deep Sea Research Part I: Oceanographic Research Papers, 57, 113-124,
859   10.1016/j.dsr.2009.09.007, 2010.

861   Stewart, G. M. and Fisher, N. S.: Bioaccumulation of polonium   210 in marine copepods,
862   Limnology and Oceanography, 48, 2011-2019, 10.4319/lo.2003.48.5.2011, 2003a.

864   Stewart, G. M. and Fisher, N. S.: Experimental studies on the accumulation of polonium-210 by
865   marine phytoplankton, Limnology and Oceanography, 48, 1193-1201,
866   10.4319/lo.2003.48.3.1193, 2003b.

868   Subha Anand, S., Rengarajan, R., Shenoy, D., Gauns, M. and Naqvi, S. W. A.: POC export
869   fluxes in the Arabian Sea and the Bay of Bengal: A simultaneous 234Th/238U and 210Po/210Pb
870   study, Marine Chemistry, https://doi.org/10.1016/j.marchem.2017.11.005, 2017.

872   Tang, Y., Castrillejo, M., Roca-Martí, M., Masqué, P., Lemaitre, N. and Stewart, G.:
873   Distributions of total and size-fractionated particulate 210Po and 210Pb activities along the
874   North Atlantic GEOTRACES GA01 transect: GEOVIDE cruise, Biogeosciences, 15, 5437-5453,
875   https://doi.org/10.5194/bg-15-5437-2018, 2018.

877   Tang, Y., Stewart, G., Lam, P. J., Rigaud, S. and Church, T.: The influence of particle
878   concentration and composition on the fractionation of 210Po and 210Pb along the North Atlantic
879   GEOTRACES transect GA03, Deep Sea Research Part I: Oceanographic Research Papers, 128,
880   42-54, 10.1016/j.dsr.2017.09.001, 2017.

882   Turekian, K. K., Nozaki, Y. and Benninger, L. K.: Geochemistry of Atmospheric Radon and
883   Radon Products, Annual Review of Earth and Planetary Sciences, 5, 227-255,
884   10.1146/annurev.ea.05.050177.001303, 1977.

886   Verdeny, E., Masqué, P., Garcia-Orellana, J., Hanfland, C., Kirk Cochran, J. and Stewart, G. M.:
887   POC export from ocean surface waters by means of 234Th/238U and 210Po/210Pb disequilibria:
888   A review of the use of two radiotracer pairs, Deep Sea Research Part II, 56, 1502-1518,
889   10.1016/j.dsr2.2008.12.018, 2009.

891   Verdeny, E., Masqué, P., Maiti, K., Garcia-Orellana, J., Bruach, J. M., Mahaffey, C. and
892   Benitez-Nelson, C. R.: Particle export within cyclonic Hawaiian lee eddies derived from 210Pb–
893   210Po disequilibrium, Deep Sea Research Part II: Topical Studies in Oceanography, 55, 1461-
894   1472, 10.1016/j.dsr2.2008.02.009, 2008.

896   Villa-Alfageme, M., Soto, F. C., Ceballos, E., Giering, S. L. C., Le Moigne, F. A. C., Henson, S.,
897   Mas, J. L. and Sanders, R. J.: Geographical, seasonal, and depth variation in sinking particle
898   speeds in the North Atlantic, Geophysical Research Letters, 43, 8609-8616,
899   doi:10.1002/2016GL069233, 2016.

900

901 Waite, A. M., Stemmann, L., Guidi, L., Calil, P. H. R., Hogg, A. M. C., Feng, M., Thompson, P.
902 A., Picheral, M. and Gorsky, G.: The wineglass effect shapes particle export to the deep ocean in
903 mesoscale eddies, Geophysical Research Letters, 43, 9791-9800, doi:10.1002/2015GL066463,
904 2016.

905

906 Wei, C. L., Lin, S. Y., Sheu, D. D. D., Chou, W. C., Yi, M. C., Santschi, P. H. and Wen, L. S.:
907 Particle-reactive radionuclides 234Th, 210Pb, 210Po as tracers for the estimation of export
908 production in the South China Sea, Biogeosciences, 8, 3793-3808, 2011.

909

910 Wei, C. L., Yi, M. C., Lin, S. Y., Wen, L. S. and Lee, W. H.: Seasonal distributions and fluxes of
911 210Pb and 210Po in the northern South China Sea, Biogeosciences, 11, 6813-6826, 2014.

912

913 Weller, R. A. and Plueddemann, A. J.: Observations of the vertical structure of the oceanic
914 boundary layer, Journal of Geophysical Research: Oceans, 101, 8789-8806, 10.1029/96JC00206,
915 1996.

916

917 Yang, W., Guo, L., Chuang, C., Schumann, D., Ayranov, M. and Santschi, P. H.: Adsorption
918 characteristics of 210Pb, 210Po and 7Be onto micro-particle surfaces and the effects of
919 macromolecular organic compounds, Geochimica et Cosmochimic Acta, 107 47-64, 2013.

920

921 Zunino, P., Lherminier, P., Mercier, H., Daniault, N., Garcia-Ibanez, M. I. and Pérez, F. F.: The
922 GEOVIDE cruise in May-June 2014 revealed an intense MOC over a cold and fresh subpolar
923 North Atlantic, Biogeosciences, 2018.

924
925

St.	Sampling date	Basin	Integration Depth (m)				w_{20} (10^{-6} m s^{-1})				Production (mmol C m^{-2} d^{-1})			
			MLD	$Z_{1\%}$	PPZ	ThEq	MLD	$Z_{1\%}$	PPZ	ThEq	PP	±	NPP	±
1	5/19/14	Iberian Basin	15	40	136	90	-1±5	-1±4	-3±2	-2±6	33	2	69	43
13	5/24/14	Iberian Basin	35	40	90	110	0.1±3.1	0.1±3.1	-2±5	0.4±54.6	79	3	61	32
21	5/31/14	Western European Basin	15	32	64	110	-1±2	-1±4	-1±5	0.1±5	135	2	109	112
26	6/4/14	Western European Basin	30	30	98	100	-2±3	-2±2	-5±5	-5±4	174	19	58	57
32	6/7/14	Iceland Basin	30	31	70	120	-1±9	-1±9	-4±20	-3±20	105	11	48	36
38	6/10/14	Iceland Basin	30	30	69	80	1±3	1±3	3±4	3±5	68	7	44	37
44	6/13/14	Irminger Basin	26	22	44	40	1±2	1±2	2±3	2±3	137	2	46	44
60	6/18/18	Irminger Basin	17	20	36	100	-14±20	-14±20	-36±40	-11±70	166	32	50	51
64	6/19/14	Labrador Basin	20	47	80	80	2±6	7±7	3±7	3±7	54	18	47	49
69	6/22/14	Labrador Basin	20	28	44	40	-2±1	-2±3	-2±3	-2±3	27	5	46	56
77	6/26/14	Labrador Basin	15	20	59	80	4±5	4±7	7±10	9±20	80	21	50	56

Table 2. The total [210]Po flux as the sum of the flux calculated from the deficit and vertical advection, together with POC/[210]Po ratios in particles > 1 μm (derived from the power law function in Fig. 5) and POC fluxes derived from [210]Po at the corresponding depths. The uncertainties of [210]Po export flux are associated with the activity uncertainty of the radionuclides. The error for the calculated particulate POC/[210]Po ratio in each basin is the standard error of regression. The uncertainties of the [210]Po-derived POC flux were estimated based on the propagation of error. (Editors/Reviewers please NB: This is a table with 53 columns that has been divided into 3 pieces for review purposes, but which should be published as one long table.)

St.	Integration Depth (m)				^{210}Po flux (dpm m^{-2} d^{-1}): ^{210}Po/^{210}Pb term								^{210}Po flux (dpm m^{-2} d^{-1}): vertical advection term							
	MLD	$Z_{1\%}$	PPZ	ThEq	MLD	±	$Z_{1\%}$	±	PPZ	±	ThEq	±	MLD	±	$Z_{1\%}$	±	PPZ	±	ThEq	±
1	15	40	136[a]	90[a]	1.1	0.3	1.5	0.8	-4.5	2.2	-0.9	1.6	2.4	19.7	3.6	14.7	6.8	4.8	4.6	16.2
13	35[a]	40	90[a]	110[a]	3.4	0.9	4.1	0.9	4.3	1.8	3.7	2.0	-0.2	5.2	-0.2	5.6	3.7	10.0	1.0	10.6
21	15	32[a]	64[a]	110[a]	-0.6	0.5	-0.7	0.8	2.2	1.2	3.5	1.8	-1.1	4.0	-0.4	1.7	2.7	9.9	0.01	0.40
26	30	30	98[a]	100	4.8	1.5	4.8	1.5	15.2	3.1	26.4	4.8	-0.9	3.2	-0.9	3.2	4.0	4.0	2.8	4.0
32	30	31[a]	70[a]	120[a]	4.7	0.9	4.8	0.9	9.1	1.4	8.5	2.2	-1.6	12.2	-1.6	12.0	7.9	33.4	3.0	23.3
38	30	30	69[a]	80	-0.5	1.3	-0.5	1.3	3.7	2.5	5.2	2.6	0.4	1.8	0.4	1.8	-1.0	3.5	-0.9	4.9
44	26[a]	22[a]	44[a]	40	1.5	1.0	1.0	1.0	4.2	1.4	3.6	1.4	0.9	2.1	1.1	2.5	0.9	2.2	1.5	2.8
60	17[a]	20	36[a]	100	3.1	1.1	3.8	1.1	9.8	1.6	37	5.4	-24.9	49.6	-40.4	74.9	-36.2	69.0	14.1	87.1
64	20[a]	47[a]	80	80	5.8	0.8	9.8	2.1	17.8	3.2	18	3.2	-0.7	2.9	-4.3	8.8	-0.5	3.7	-0.5	3.7
69	20[a]	28[a]	44[a]	40	4.0	0.7	6.1	0.8	8.5	1.6	8.3	1.5	1.9	3.3	3.4	5.8	5.8	7.9	6.7	8.9
77	15[a]	20	59[a]	80	2.2	0.6	2.9	0.7	7.0	2.4	9.8	2.9	-0.6	5.2	0.3	6.4	3.0	9.9	-15	29

[a]For the depths at which total radionuclides data are not available, the measured values of total [210]Po and ^{210}Pb activities were linearly interpolated at the missing depths.

31

946   Table 2. (continued)
947

St.	^{210}Po flux (dpm m^{-2} d^{-1}): total flux								POC/^{210}Po (μmol dpm^{-1})							
	MLD	±	$Z_{1\%}$	±	PPZ	±	ThEq	±	MLD	±	$Z_{1\%}$	±	PPZ	±	ThEq	±
1	3.5	19.7	5.1	14.7	2.3	5.3	3.6	16.2	540	67	305	67	150	67	190	67
13	3.2	5.3	3.9	5.7	7.9	10.1	4.7	10.8	330	67	305	67	190	67	169	67
21	-1.7	4.1	-1.1	1.8	4.9	10.0	3.5	1.9	542	89	389	89	287	89	227	89
26	3.9	3.5	3.9	3.5	17.7	5.1	29.2	6.2	400	89	400	89	238	89	236	89
32	3.0	12.2	3.2	12.1	17.0	33.4	11.6	23.4	367	111	363	111	265	111	216	111
38	-0.2	2.3	-0.2	2.3	2.7	4.3	4.2	5.6	367	111	367	111	267	111	252	111
44	2.5	2.3	2.1	2.7	5.1	2.6	5.1	3.1	310	107	330	107	254	107	263	107
60	-21.8	49.6	-36.6	74.5	-26.4	69.0	51.2	87.2	364	107	342	107	274	107	187	107
64	5.1	3.0	5.5	9.0	17.4	4.9	17.4	4.9	675	152	375	152	261	152	261	152
69	5.9	3.4	9.4	5.8	14.4	8.0	15.0	9.0	675	152	536	152	393	152	419	152
77	1.5	5.2	3.1	6.4	10.1	10	-4.8	29.0	822	152	675	152	321	152	261	152

948
949

32

950 Table 2. (continued)

951

| St.	^{210}Po-POC flux (mmol C m^{-2} d^{-1}): ^{210}Po/^{210}Pb term								^{210}Po-POC flux (mmol C m^{-2} d^{-1}): total flux							
	MLD	±	$Z_{1\%}$	±	PPZ	±	ThEq	±	MLD	±	$Z_{1\%}$	±	PPZ	±	ThEq	±
1	0.6	0.2	0.4	0.3	-0.7	0.4	-0.2	0.3	1.9	10.7	1.5	4.5	0.3	0.8	0.7	3.1
13	1.1	0.4	1.3	0.4	0.8	0.4	0.6	0.4	1.0	1.8	1.2	1.7	1.5	2.0	0.8	1.9
21	-0.3	0.3	-0.3	0.3	0.6	0.4	0.8	0.5	-0.9	2.2	-0.4	0.7	1.4	2.9	0.8	0.5
26	1.9	0.7	1.9	0.7	3.6	1.5	6.2	2.6	1.5	1.4	1.5	1.4	4.6	2.0	6.9	3.0
32	1.7	0.6	1.7	0.6	2.4	1.1	1.8	1.1	1.1	4.5	1.1	4.4	4.5	9.1	2.5	5.2
38	-0.2	0.5	-0.2	0.5	1.0	0.8	1.3	0.9	-0.1	0.8	-0.1	0.8	0.7	1.2	1.1	1.5
44	0.5	0.4	0.3	0.4	1.1	0.6	1.0	0.5	0.8	0.8	0.7	0.9	1.3	0.9	1.4	1.0
60	1.1	0.5	1.3	0.5	2.7	1.1	6.9	4.1	-7.9	20	-12.5	25.9	-7.2	19.1	9.6	17.2
64	3.9	1.0	3.7	1.7	4.7	2.8	4.7	2.8	3.5	2.1	2.1	3.5	4.5	2.9	4.5	2.9
69	2.7	0.8	3.3	1.0	3.4	1.4	3.5	1.4	4.0	2.5	5.1	3.4	5.7	3.8	6.3	4.4
77	1.8	0.6	1.9	0.6	2.3	1.3	2.5	1.7	1.3	4.3	2.1	4.3	3.2	3.6	-1.3	7.6

952 Table 3. The ratio of POC concentration to ^{210}Po activity (POC/^{210}Po) in the ~~in-situ pumped~~

953 particles collected by in situ pumps. SSF: small size fraction (1-53 μm); LSF: large size fraction

954 (> 53 μm); ~~TSF~~TPF: total ~~size~~ particulate fraction (> 1 μm).

955

Station	Depth (m)	POC/^{210}Po (μmol dpm^{-1})					
		SSF	±	LSF	±	~~TSF~~TPF	±
1	30	276	32	414	58	296	30
1	80	166	28	1040	159	355	44
1	550	41	4	31	4	39	4
1	800	18	17	19	4	19	10
1	120	108	14	222	42	117	13
1	250	65	7	63	9	65	6
13	60	289	29	216	26	281	25
13	100	206	20	132	14	198	17
13	200	79	7	50	8	76	7
13	450	73	7	35	7	69	6
21	80	622	51	13405	2599	1280	96
21	120	133	18	2398	407	380	44
21	250	85	9	482	133	109	10
21	450	54	6	117	14	60	6
26	30	377	70	310	34	350	42
26	83	271	41	289	37	280	28
26	153	275	94	118	14	209	43
26	403	67	21	43	19	62	17
32	30	492	60	733	382	500	59
32	60	379	43	337	87	376	40
32	100	311	39	376	56	326	33
32	200	145	17	133	30	144	15
32	450	41	5	55	9	42	4
32	800	25	4	55	7	29	4
38	20	254	38	345	108	258	37
38	60	339	51	284	66	333	46
38	109	157	15	196	23	163	13
44	20	1025	115	3085	798	1176	124
44	40	463	58	1379	1787	475	59
44	80	140	14	90	23	137	13
44	150	102	18	97	56	102	17
44	300	47	7	25	7	45	6
60	8	306	30	1003	150	422	36

60	60	232	33	851	193	272	36
60	100	197	33	303	72	209	31
60	250	61	7	294	84	72	8
64	30	525	77	656	83	580	58
64	60	455	75	286	77	434	64
64	100	439	49	319	44	420	41
64	150	107	36	158	28	129	24
64	400	40	5	48	8	41	4
69	20	347	44	879	164	397	46
69	60	78	6	657	216	84	7
69	100	257	26	359	44	268	24
69	150	125	14	127	25	125	13
69	410	30	3	71	8	34	3
77	10	1281	309	917	150	1181	213
77	50	1372	357	1020	412	1339	320
77	80	512	63	544	103	516	57
77	200	84	13	217	79	92	13
77	460	22	3	59	6	27	3

956
957

35
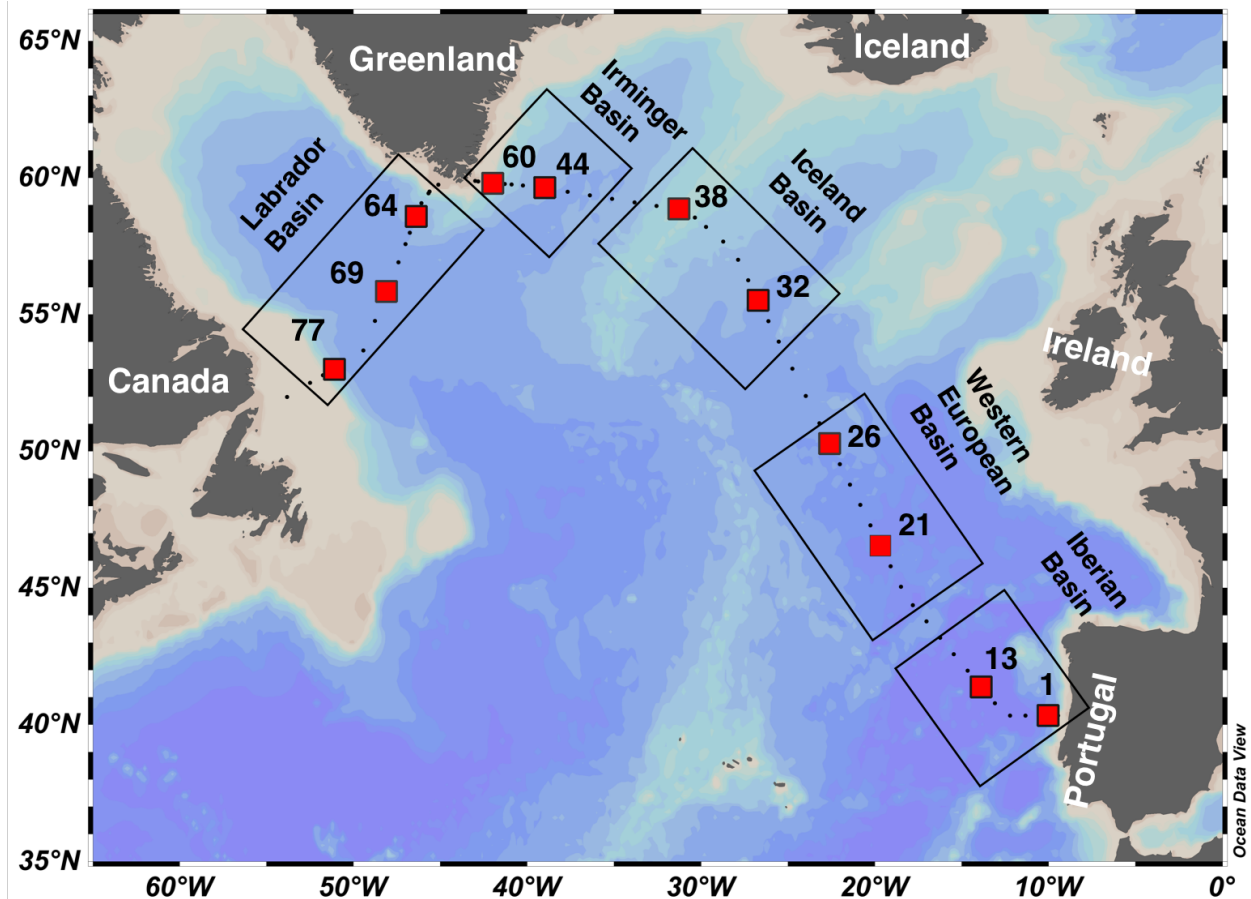
963 Fig. 1. Map of stations occupied during the GA01 transect in the North Atlantic. The red squares
964 indicate the stations where ^{210}Po and ^{210}Pb activities were measured discussed in this study. The
965 transect is divided into the Iberian Basin (stations 1, 13), the Western European Basin (stations
966 21, 26), the Iceland Basin (stations 32, 38), the Irminger Basin (stations 44, 60), and the
967 Labrador Basin (stations 64, 69, 77).
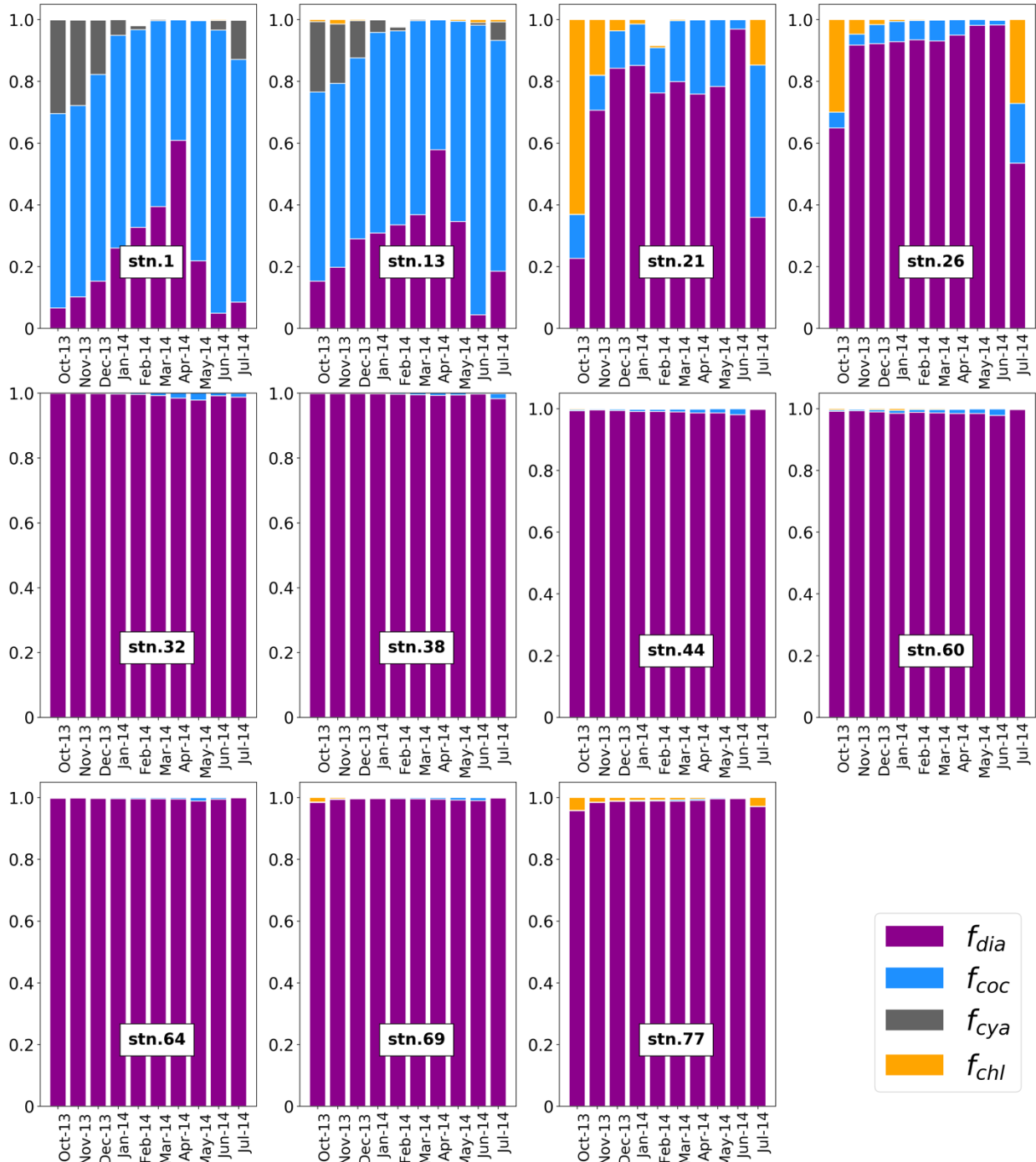
972
973
974 Fig. 2. Satellite-derived monthly average fraction of major phytoplankton groups from October

975 2013 to July 2014 along the GA01 transect: $f_{dia}, f_{coc}, f_{cya},$ and f_{chl} are the fraction of diatoms

976 (purple), coccolithophores (blue), cyanobacteria (gray), and chlorophytes (orange), respectively.

977 Data are from the Giovanni online data system https://giovanni.gsfc.nasa.gov/giovanni/.

978
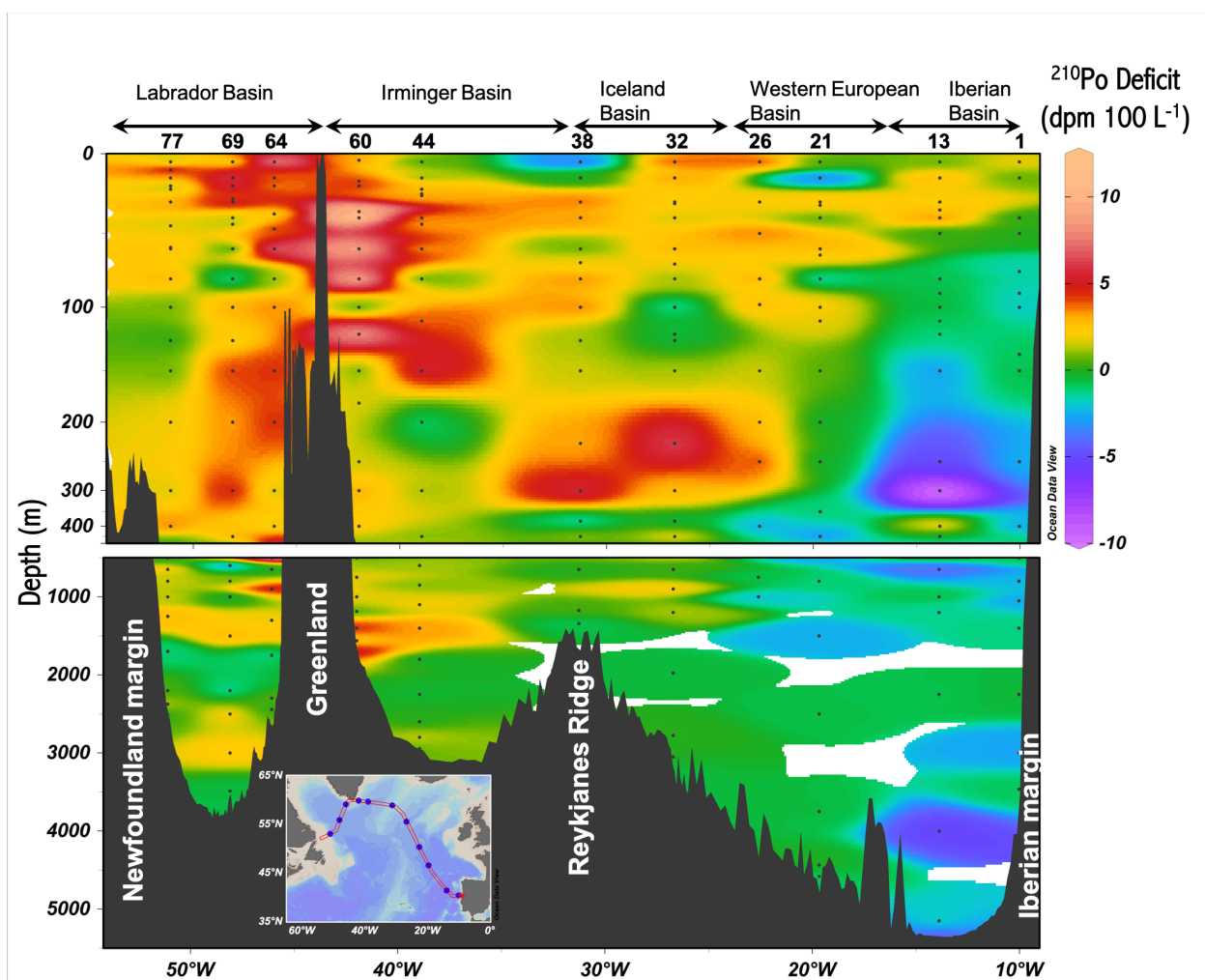
Fig. 3. Section plots of water column ^{210}Po deficits (dpm 100 L^{-1}, total ^{210}Pb activity minus total ^{210}Po activity) across the GA01 transect. Upper panel is the upper 500 m. Lower panel is 500 – 5500 m. Station numbers and basins are shown on the top of the upper panel.

986
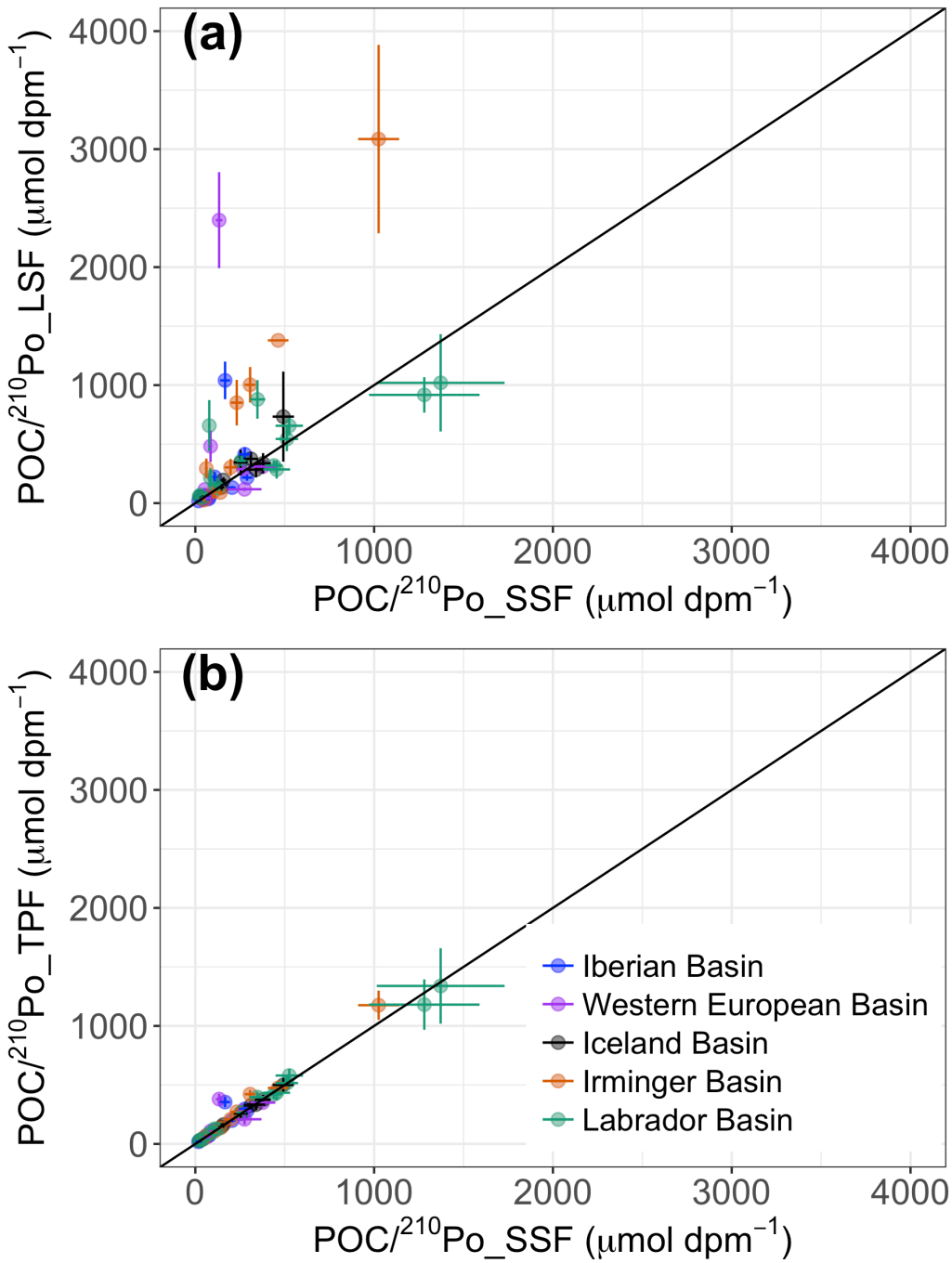
Fig. 4. Plots of the ratios of POC concentration to ^{210}Po activity in: (a) the large (> 53 μm) particles (POC/^{210}Po_LSF) against the small (1-53 μm) particles (POC/^{210}Po_SSF), and in (b) the total (> 1 μm) particles (POC/^{210}Po_TPF) against the small particles. The black lines indicate the 1:1 line.
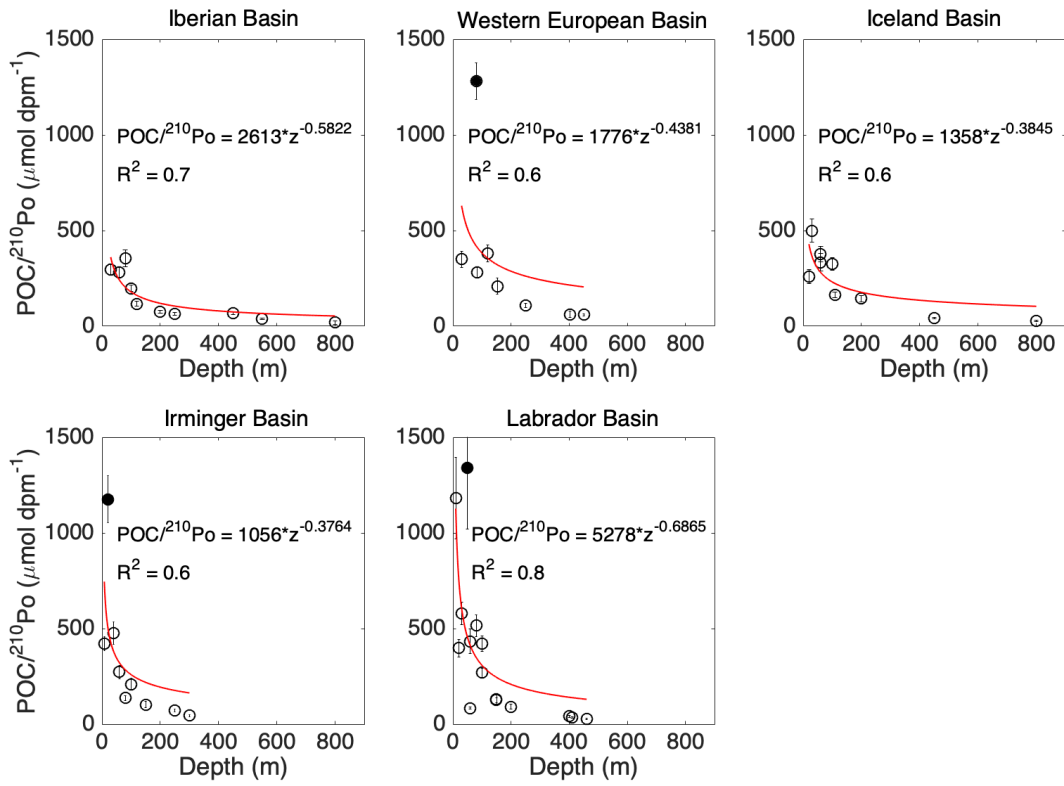
Fig. 5. The ratios of POC concentration to ^{210}Po activity in the total particles vs. depth in each basin along the GA01 transect. Power law regression (red line) was fitted for POC/^{210}Po against depth in each plot: the Iberian Basin (stations 1, 13), West European Basin (stations 21, 26), Iceland Basin (stations 32, 38), Irminger Basin (stations 44, 60), and Labrador Basin (stations 64, 69, 77). The data points denoted as filled black circles were outliers (points at a distance greater than 1.5 standard deviations from the power law model) and excluded from the power law regression.
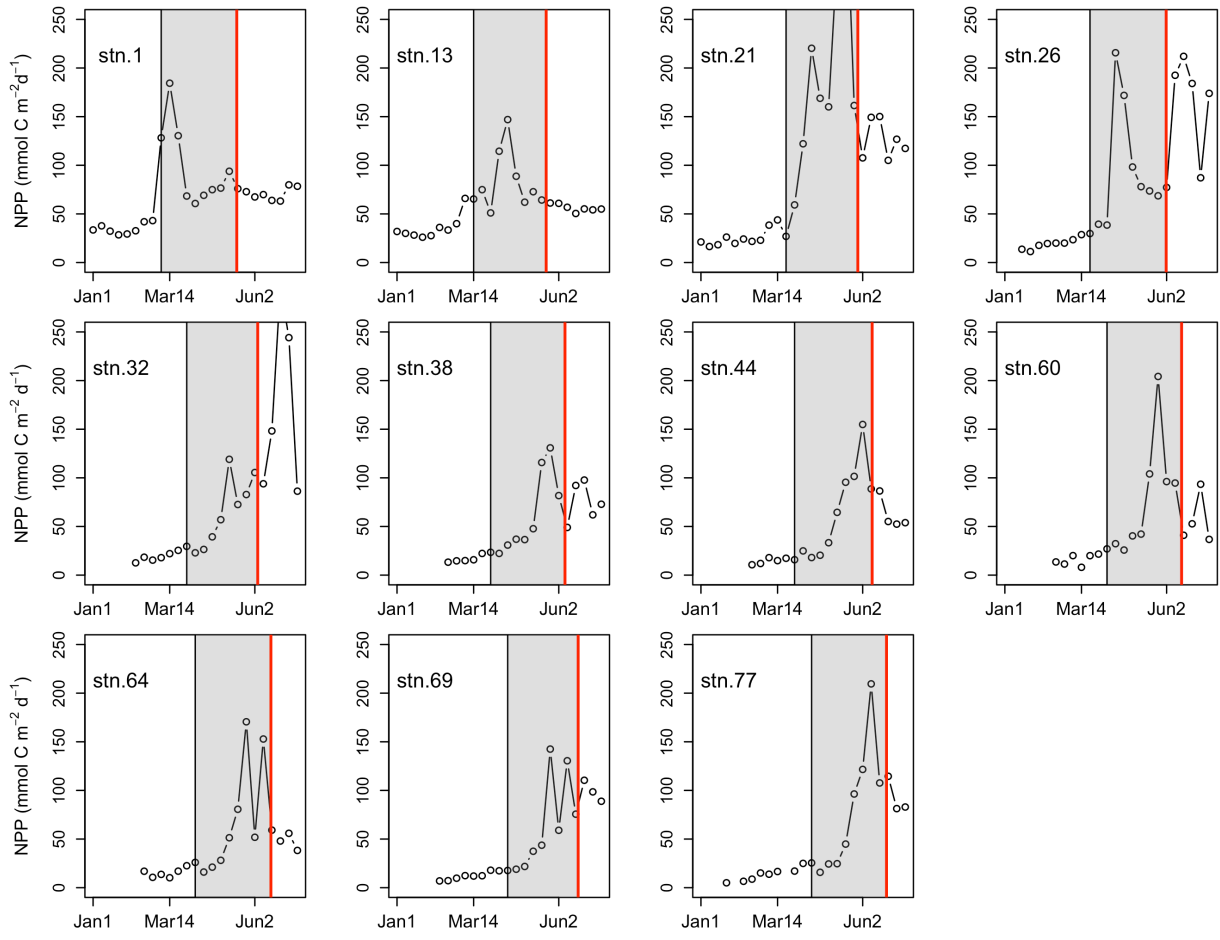
1000
1001

Fig. 67. Time-series (January 1- July 12, 2014) satellite estimates of net primary production (NPP) between January 1 and July 12 in 2014 at each station along the GA01 transect (NPP, VPGM algorithm, http://www.science.oregonstate.edu/ocean.productivity/). The shading rectangle in each plot denotes NPP for about 2 months prior to the sampling date. Two months NPP data is needed because such a time scale could ensure the sensitivity for NSS estimates (Friedrich and Rutgers van der Loeff, 2002; Stewart et al., 2007). The vertical red line in each plot indicates the sampling date at each station.

1010
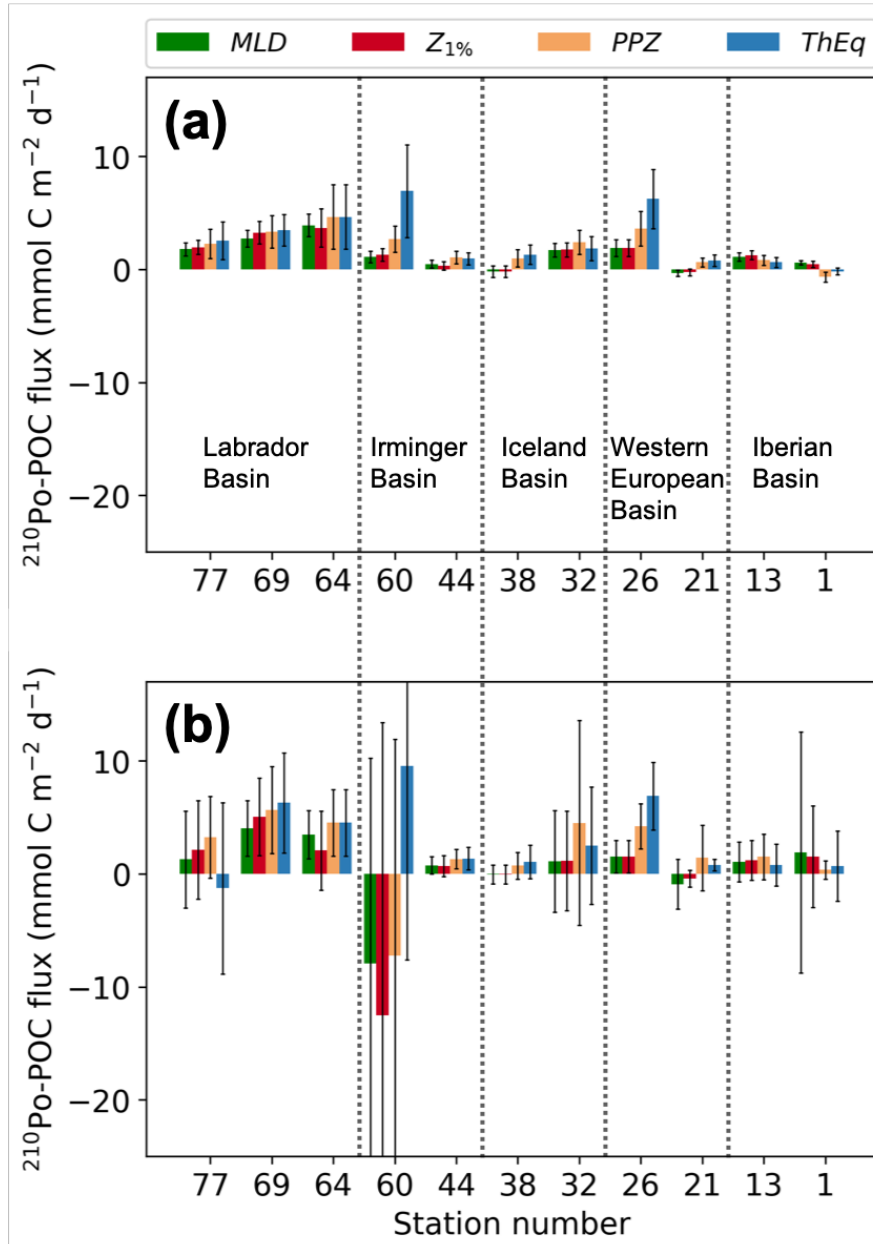
Fig. 76. POC fluxes derived from ^{210}Po for the mixed layer depth (MLD), the base of the euphotic zone ($Z_{1\%}$), the base of the primary production zone (PPZ), and the ^{234}Th-^{238}U equilibrium depth (ThEq). (a) POC fluxes derived from the ^{210}Po fluxes that were calculated from the deficit alone; (b) POC fluxes derived from the sum of the ^{210}Po fluxes that were calculated from the ^{210}Po deficit and vertical advective flux. Note that the > 1 μm particles were used to calculate the POC/^{210}Po ratios. The stations were plotted from west to east.
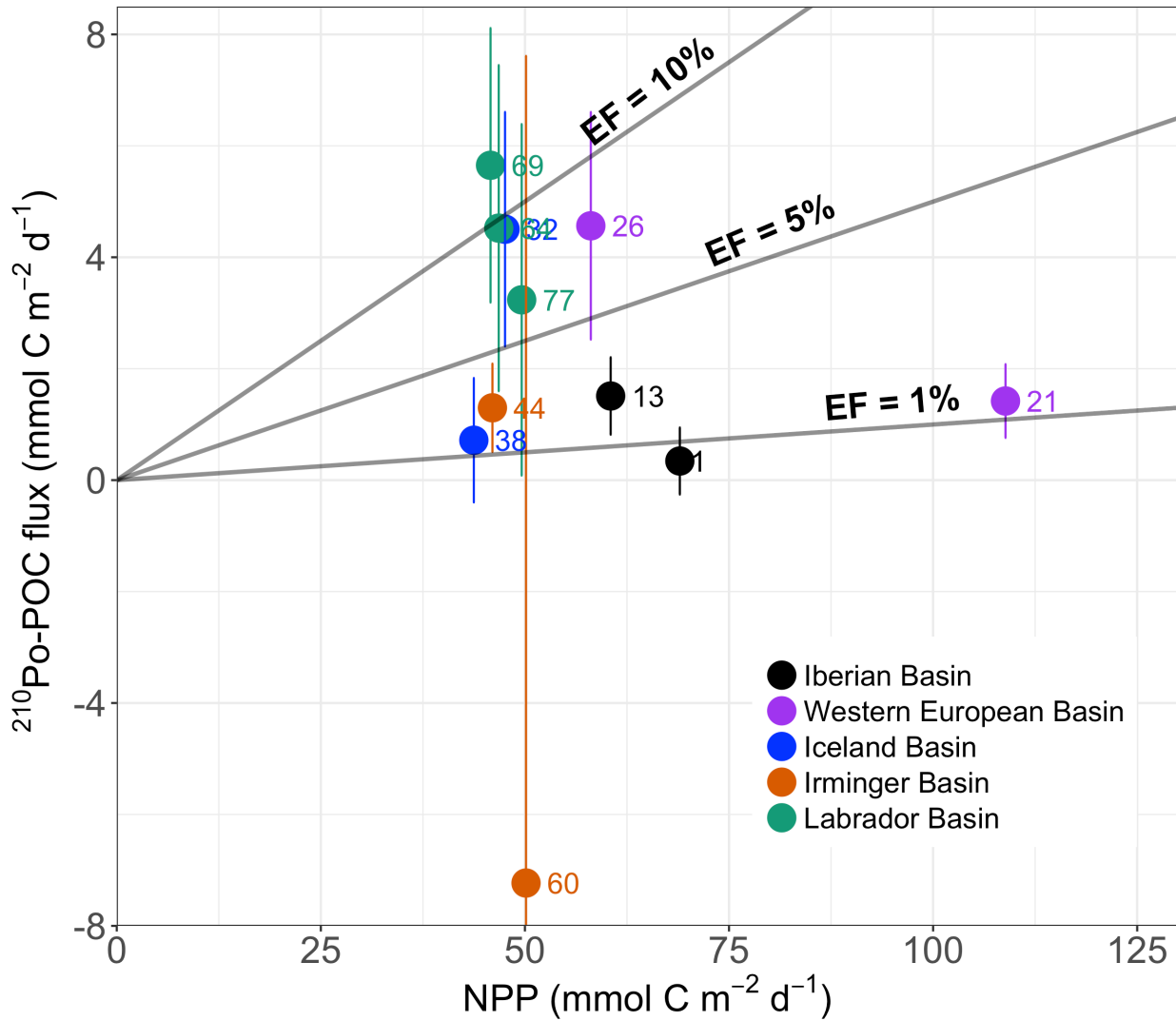
Fig. 8. Plot of POC export flux derived from ^{210}Po method (^{210}Po-POC) versus satellite estimates of net primary production (NPP). The NPP values were averaged for the previous 138 days (^{210}Po half-life) prior to the sampling date. The sum of the ^{210}Po fluxes calculated from the ^{210}Po deficit and vertical advective flux, and the POC/^{210}Po ratios in the > 1 μm particles were used to derive POC fluxes. The ^{210}Po-POC fluxes were integrated within the primary production zone (PPZ). Lines of export efficiency (EF) of 10%, 5%, and 1% are drawn in the plot. The numbers in the plot are labelled as station numbers. The color codes of the stations correspond to the basins.
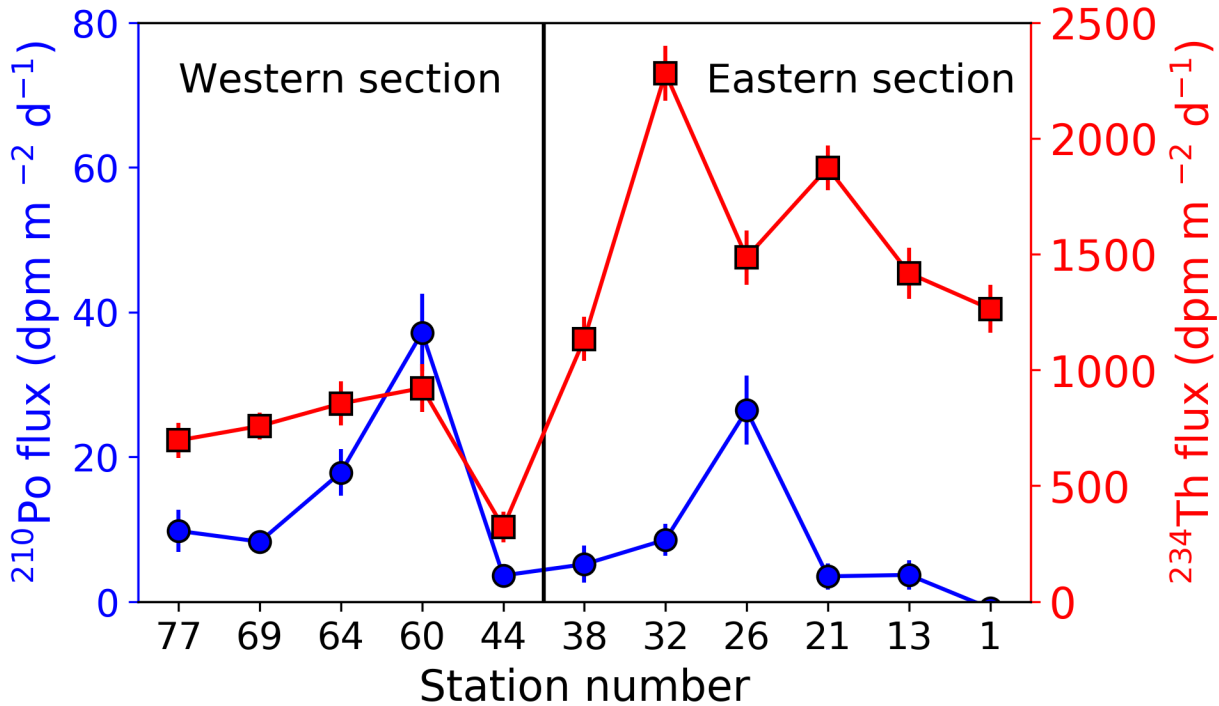
Fig. 9. Sinking fluxes of [210]Po (blue circles) and [234]Th (red squares) integrated to the depth where [234]Th activity returned to equilibrium with [238]U activity (ThEq) assuming steady state and negligible physical transport along the GA01 transect. Note that the stations are plotted from west to east, ~~which is opposite the cruise track from Portugal to Canada,~~ and the transect was separated into the western (stations 44 - 77) and eastern (stations 1 - 38) sections.
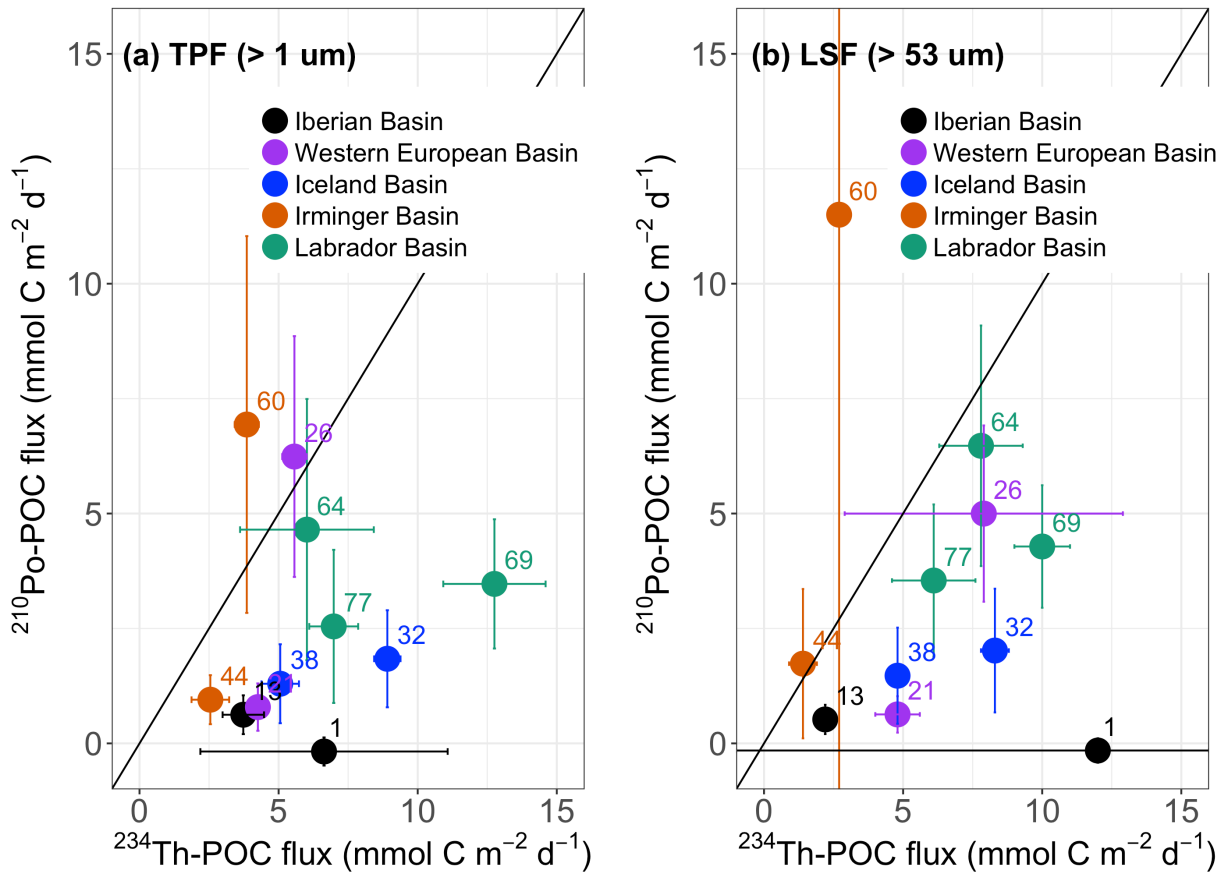
Fig. 10. Plot of the POC flux derived from ^{210}Po (^{210}Po-POC) versus the POC flux derived from ^{234}Th (^{234}Th-POC) at 11 stations along the GA01 transect. Both the fluxes of ^{210}Po and ^{234}Th were calculated from the deficit term alone assuming steady state and negligible physical transport. The POC/radionuclide ratios on (a) total particulate fraction (TPF, ~~particles~~ > 1 μm) and (b) large size fraction (LSF, > 53 μm) were used to calculate the POC flux. The fluxes were integrated down to the depth where ^{234}Th activity returned to equilibrium with ^{238}U activity (ThEq). The numbers in the plot are station numbers. The color codes of the stations correspond to the basins.